# A Novel *in vitro* Model for Mature *Toxoplasma gondii* Bradyzoites Reveals their Metabolome and a Diminished Role of the Mitochondrial Tricarboxylic Acid Cycle

**Authors**

Céline Christiansen[1], Deborah Maus[1], Florian Melerowicz[1], Jana Scholz[1], Mateo Murillo-León[4,5,6], Tobias Steinfeldt[4,5], Tobias Hoffmann[2], Frank Seeber[3], Martin Blume[1,7 *]

1 NG2: Metabolism of Microbial Pathogens, Robert Koch-Institute, 13353, Berlin, Germany
2 ZBS 4: Advanced Light and Electron Microscopy, Centre for Biological Threats and Special Pathogens 4, Robert Koch-Institute, 13353, Berlin, Germany
3 FG 16: Mycotic and Parasitic Agents and Mycobacteria, Robert Koch-Institute, 13353, Berlin, Germany
4 Institute of Virology, Medical Center University of Freiburg, 79104 Freiburg, Germany.
5 Faculty of Medicine, University of Freiburg, 79104 Freiburg, Germany.
6 Faculty of Biology, University of Freiburg, 79104 Freiburg, Germany.
7 Lead contact
* Corresponding author

Martin Blume
Junior Group 2
Robert Koch-Institute
Seestr. 10
13353 Berlin
Germany
Email: blumem@rki.de

**Highlights**

- *Toxoplasma gondii* forms mature tissue cysts in immortalized human myotubes
- *In vitro* cysts of *T. gondii* develop drug tolerance and temperature stress resistance
- Untargeted metabolomic characterization of tissue cysts reveals a distinct metabolome
- The mitochondrial tricarboxylic acid cycle is dispensable in *T. gondii* bradyzoites

**Summary**

The apicomplexan parasite *Toxoplasma gondii* causes chronic and drug-tolerant infections, yet current models do not permit metabolomic characterization of these persisting tissue cysts. Here, we developed a human myotube-based *in vitro* culture model of functionally mature tissue cysts that enabled direct measurements of their metabolome. The cysts are functionally mature and tolerate exposure to a range of antibiotics and to extended temperature stresses and are orally infectious to mice. Metabolomic characterization of purified cysts reveals global changes that comprise systematically increased levels of amino acids and decrease abundance of nucleobase- and tricarboxylic acid cycle-associated metabolites. Consequently, pharmacological modulation of the TCA cycle in *T. gondii* bradyzoites reveals that this pathway is rendered dispensable during parasite stage conversion. Direct access to persisting parasite stages will be essential for the dissection of functionally important host-parasite interactions and drug evasion mechanisms and also help to identify new strategies for therapeutic intervention.

## Introduction

*Toxoplasma gondii* is an apicomplexan parasite that infects most warm-blooded animals, including an estimated third of all humans (Tenter et al., 2000). Similar to other infectious protozoa, including the apicomplexan *Plasmodium vivax* and the kinetoplastidae *Trypanosoma cruzi* and *Leishmania* spp., *T. gondii* forms specialized persistent stages that resist immune responses and many medical treatments (Barrett et al., 2019). *T. gondii* bradyzoites reside, surrounded by a glycan-rich cyst wall, in brain and muscle tissue and can be transmitted through ingestion of undercooked meat products (Desmonts et al., 1965). These largely asymptomatic infections can cause recurring disease in immune-weakened individuals that are lethal if untreated (Luft et al., 1984).

The rapid proliferation of tachyzoites and the slow replication or dormancy of bradyzoites exert distinct demands on the metabolism of *T. gondii*. The rate of proliferation and the metabolic state are closely interrelated. They have been shown to independently affect lethality of antibiotics against bacterial microbes, with metabolism being the dominant factor (Lopatkin et al., 2019). While multiple metabolomic investigations on the tachyzoite stage of *T. gondii* revealed unexpected features of key metabolic pathways such as the GABA-shunt of the tricarboxylic acid (TCA) cycle, a constitutively active gluconeogenic fructose 1,6-bisphosphatase and the presence of a non-oxidative pentose phosphate pathway (Blume et al., 2015; MacRae et al., 2012; Olson et al., 2020), the metabolism of bradyzoites has only been characterized indirectly (Blume and Seeber, 2018), largely due to experimental constraints. In contrast to tachyzoites, bradyzoites depend on the turnover of the storage polysaccharide amylopectin by glycogen phosphorylase (Murata et al., 2017), the hexose kinase (Shukla et al., 2018) and on a dedicated isoform of lactate dehydrogenase (Abdelbaset et al., 2017). This indicates that glycolytic degradation of glucose plays an important role in bradyzoites. Similarly, the relevance of mitochondrial and amino acid metabolism has been inferred. Bradyzoite formation is induced by a number of electron transport inhibitors, including atovaquone, rotenone, oligomycin and antimycin (Ferreira da Silva Mda et al., 2008; Tomavo and Boothroyd, 1995). Moreover, *T. gondii* cysts survive extended atovaquone exposure *in vivo* (Araujo et al., 1991; Ferguson et al., 1994b), indicating that their mitochondrial electron transport chain is not strictly essential. Similarly, bradyzoites can also be induced by limiting supply of exogenous amino acids (Ferreira da Silva Mda et al., 2008) and their viability depends on proteolysis in their plant-like vacuolar compartment (Di Cristina et al., 2017) and on autophagy (Smith et al., 2020). Collectively, these data indicate a substantial remodeling of metabolic homeostasis in bradyzoites as a strategy to cope with nutrient limitations (Lüder and

Rahman, 2017). This proposed metabolic shift may also be associated with tolerance against many antiparasitic treatments, as the metabolic state of microbes has important implications for the lethality of antimicrobials (Lopatkin et al., 2019).

However, our ability to investigate such mechanisms remains very limited by the lack of adequate *in vitro* culture models (Barrett et al., 2019). Current methods to experimentally generate mature *T. gondii* tissue cysts are confined to murine infections with cystogenic *T. gondii* strains (Ferguson and Hutchison, 1987; Watts et al., 2015). The number of obtainable cysts from this *in vivo* model are low, precluding their metabolic analysis with current mass spectrometry-based approaches. In contrast, *in vitro* models are scalable and the stage conversion of *T. gondii* can be induced by a variety of treatments, such as alkaline, heat and chemical stress (Soete et al., 1994), nutrient starvation (Fox et al., 2004), excess adenosine (Mahamed et al., 2012), inhibitors of parasite protein kinases (Donald et al., 2002) as well as host cell-dependent factors such as cell cycle arrest and low glycolytic flux (Lüder and Rahman, 2017; Mayoral et al., 2020; Weilhammer et al., 2012). In addition, the infection of C2C12 murine skeletal muscle cells and neurons (Guimarães et al., 2009; Guimaraes et al., 2008) facilitates spontaneous stage conversion of cystogenic strains. Generally, maturation times of cysts *in vitro*-cysts remain brief but cysts develop detectable tolerance against short exposure to low doses of pyrimethamine after three days (Murata et al., 2017) and become orally infectious to mice at high doses after five days of culture (Fux et al., 2007). However, establishment of long-term cultures that allow development of pan-antimicrobial- and temperature stress-tolerant cysts (Dubey et al., 1990; Dunay et al., 2018) remains a challenge. Incomplete differentiation leads to expansion of proliferating parasite populations and subsequent host cell lysis that limits the scale and duration of current *in vitro* culture systems.

Here, we developed a human myotube-based *in vitro* culture system that is scalable and enables long-term maturation of *T. gondii* cysts. The cysts resemble *in vivo* cysts in their ultrastructure, tolerance to antiparasitics and temperature stress and infectiousness to mice. Mass spectrometry-based metabolic profiling revealed a distinct metabolome exhibiting an active but dispensable TCA cycle.

## Results

### KD3 human myoblasts differentiate into multinucleated myotubes

*T. gondii* persists in skeletal muscle tissue (Dubey, 1988), but robust *in vitro* culture systems supporting long-term maturation of tissue cysts in these natural host cells are lacking. We tested an immortalized human skeletal muscle cell isolate (KD3) (Shiomi et al., 2011) for its ability to support the culture of *T. gondii* tissue cysts. Sub-confluent myoblast cultures were differentiated into myotubes through serum starvation for five days until cells fused to multinucleated tubes that were expressing myosin heavy chain (Fig. 1A) and developed spontaneous contraction activity (Video S1) (Shiomi et al., 2011). Accordingly, the myogenic index, which reflects the fraction of total nuclei that reside in multinucleated cells, rose to 0.3 (Fig. 1B).

### KD3 human myotubes support development of matured cysts of several *T. gondii* strains

Next, KD3 myotubes were tested for their ability to support long-term maturation of *T. gondii* cysts. We infected myotubes with Pru-tdTomato parasites, a type II Prugniaud strain constitutively expressing the tandem (td) Tomato variant of the red fluorescent protein, for up to 21 days. Evaluation of the ultrastructure of the encysted parasites by electron microscopy (Fig. 2A, S1) revealed hallmarks of bradyzoites including abundant amylopectin granules to posterior positioned nuclei after seven days of infection. The formation of the cyst wall is indicated by the apparent deposition of electron-dense vesicular-tubular material along the parasitophorous vacuolar membrane throughout the course of infection (Fig S1D) (Speer et al., 1999).

*T. gondii* strains differ greatly in their capacity to form tissue cysts *in vitro* and *in vivo* (Sullivan et al., 2009) and their maturation is accompanied by sequential regulation of marker protein expression (Ferguson, 2004). To test the suitability of KD3 myotubes to culture tissue cysts of multiple *T. gondii* strains, we monitored the formation of tissue cysts of eight parasite strains of three major isotypes under $CO_2$-deplete conditions at neutral and basic pH. Stage conversion was detected by staining the cyst wall with *Dolichos biflorus* agglutinin (DBA) and antibodies against the CC2 protein (Gross et al., 1995) and by the absence of the tachyzoite-specific surface antigen 1 (SAG1) (Fig. 2 B). Myotubes infected with type I RH-*Δku80Δhxgprt* parasites that do not easily form tissue cysts *in vitro* served as a tachyzoite control.

Strikingly, under both conditions all cultures were DBA-positive and remained stable without being overgrown by tachyzoites for 21 days. We observed almost complete differentiation of type III VEG parasites into DBA- and CC2-positive and SAG1-negative cysts. All type II strains and the type III NED strain showed intermediate maturation (between 35 % and 63 %) that was

considerably increased in basic pH to 73 % and 83 %, respectively. Also, wild-type type I strains GT1 and RH exhibited differentiation up to 30 % that increased to 77 % and 55 % at basic pH, respectively. As expected, the high-passage laboratory strain RH*Δku80* did not differentiate at neutral pH but required basic conditions (Fig. 2C).

We also tested spontaneous stage conversion under standard bicarbonate-replete conditions as described for the murine skeletal muscle cell line C2C12 (Ferreira-da-Silva Mda et al., 2009). To this end, we infected myoblasts, myotubes and HFF cells with Pru-GFP parasites which express GFP controlled by the bradyzoite-specific LDH2 promoter (Singh et al., 2002). After three days parasites started to express GFP in a subset of vacuoles only in myotubes but not myoblasts and human foreskin fibroblast (HFF) cells (Fig. S2).

Together, these data show that KD3 myotubes enable the culture of tissue cysts of multiple parasite strains at physiological pH over the course of 21 days and augment spontaneous stage conversion.

## KD3 human myotubes support the formation of orally infectious, pepsin- and temperature stress-resistant cysts

To test whether *in vitro* cysts also develop functional hallmarks of *in vivo* cysts, such as resistance to temperature stress and pepsin digestion (Dubey et al., 1990), we infected myotubes with Pru-tdTomato parasites at MOI 0.1 and then differentiated parasites for up to 35 days (Fig. 3A). Intracellular cysts were digested with pepsin for 20, 40 and 60 min, the reaction mix was then neutralized and cysts were seeded onto HFF cells to allow re-differentiation in tachyzoite medium under $CO_2$-replete conditions. Untreated and pepsin-digested tachyzoite cultures served as positive and negative controls, respectively. Growth of both, untreated tachyzoite and bradyzoite cultures, was observed by an increase in red fluorescence (indicative of tachyzoite replication) after two and seven days, respectively (Fig. 3B). Interestingly, all pepsin-treated bradyzoite cultures recovered after 7, 9 and 14 days, depending on the length of the pepsin digest, while pepsin-digested tachyzoite cultures did not recover even after a period of 21 days. We quantified pepsin resistance across the time course of cyst maturation by calculating a resistance score (RS) (see Material and Methods) based on the pepsin-inflicted growth delay (Fig 3. C). Already after 14 days all digested cultures recovered with an RS between 0.4 to 0.5. Pepsin resistance continued to increase over the course of 28 days up to an RS of 0.8 (Fig 3. C).

In human transmission scenarios *T. gondii* tissue cysts survive extended cold-storage and heat stress (Dubey et al., 1990). To test whether *in vitro* cysts would survive under these conditions, cysts were matured for 35 days and treated with a combination of (1) storage as cell 'pellets' at 4 °C for up to seven days, (2) a 5 min heat shock at 55 °C or 65 °C and (3) pepsin digestion for 60 min (Fig. 3D). Storage at room temperature (RT) for two days served as a positive control and did not decrease viability in comparison with untreated cysts, as indicated by an RS of 1. Different combinations of storage at 4 °C for four or seven days and heat shock at 55 °C did lower the RS to a range between 0.75 and 0.65, while heating to 65 °C effectively killed tissue cysts as expected (Dubey et al., 1990). These results demonstrate that myotube-grown cysts develop traits that are important for oral transmission of tissue cysts as it occurs with cysts in muscle tissues of farm animals.

The oral infectivity to mice was also confirmed directly by inoculating groups of five mice with either 50 or 500 35-day-old *in vitro* cysts via oral gavage (Fig. 3E-F). Both inocula led to sero-conversion of mice after 30 days, as indicated by detection of *T. gondii* specific Immunoglobulin G (Fig. 3E). The infection was accompanied by a weight loss after 11 days (Fig. 3F) which was transient for mice that received 50 cysts and lasted for the duration of the experiment in mice that received 500 cysts (Fig. 3F). The presence of *T. gondii* cysts in the brains of infected mice was microscopically confirmed 30 days post infection in DBA-stained brain homogenates (Fig. S3).

In summary, these data show that myotube-generated *T. gondii* cysts are orally infectious to mice and express resistance to stress observed in a typical transmission setting to humans.

**KD3 myotube-derived tissue cysts develop resistance against antiparasitics.**

*T. gondii* tissue cysts largely resist current toxoplasmosis treatments. To test whether cysts cultured in myotubes mirror drug resistance *in vivo* we exposed 14-, 21- and 28-day-old Pru-tdTomato-expressing cysts to antiparasitics for seven days and monitored their re-differentiation into tachyzoites under $CO_2$-replete conditions as a measure of cyst viability (Fig. 4A). Figure 4B shows the fluorescence signal observed over 49 days, including 14 days of cyst maturation, seven days of pyrimethamine treatment, and 28 days of re-differentiation. Growth of DMSO- and pyrimethamine-treated parasites was indicated by an increase in fluorescence above background at 14- and 24-days post treatment, respectively (Fig. 4 B). Next, 14-, 21- and 28-day-old tissue cysts were treated with 5 µM and 20 µM pyrimethamine, 20 µM sulfadiazine and

0.1 µM of the mitochondrial bc1-complex inhibitor 1-hydroxy-2-dodecyl-4(1)-quinolon (HDQ) (Saleh et al., 2007) (Fig. 4C). All bradyzoite cultures survived all tested treatments. Interestingly, while resistance against sulfadiazine, HDQ and low doses of pyrimethamine was already fully developed after 21 days, indicated by an RS of 1, resistance against high doses of pyrimethamine increased until 28 days of maturation (Fig. 4 C). In contrast, tachyzoite-infected myotubes, which served as a control and are shown as '0 days differentiated cultures', did not survive treatment with 20 µM pyrimethamine, 20 µM sulfadiazine and 0.1 µM HDQ. However, two out of three tachyzoite cultures survived 5 µM pyrimethamine treatment, with a low RS of 0.18. Furthermore, we tested the resistance against two different bumped kinase inhibitors (BKI), BKI1553 and BKI1294 (Fig. 4D), that have been shown to decrease cyst burden in brains of infected mice (Scheele et al., 2018; Winzer et al., 2015). Consistent with previous results, tachyzoites did not grow after exposure to fourfold of the $IC_{50}$ of each compound. In contrast, already 14-day-old tissue cysts were resistant to both treatments, with an RS of 0.42 and 0.83, respectively. Resistance increased further and BKI1553 became completely ineffective against 28-day-old cysts while cysts reached an RS of 0.89 against BKI1294 (Fig. 4D).

Taken together, these data demonstrate that myotube-cultured cysts gradually develop resistance against both established and experimental antiparasitics and are suitable for efforts to screen compounds against chronically infectious forms of *T. gondii*.

**The metabolome of *T. gondii* depends on the host cell type and parasite stage**

The metabolome is directly linked to the mode of action of many antiparasitics and may also associated with their efficacy (Lopatkin et al., 2019). However, the metabolome of bradyzoites remains largely unknown. We compared the metabolome of Pru-tdTomato parasites in their bradyzoite form with intracellular tachyzoites in both HFF cells and myotubes. Parasites were differentiated into cysts for 28 days, quenched with ice-cold PBS, harvested and released from cells by repeated passages through needles. Cysts were then purified from host cell debris via binding to DBA-coated magnetic beads. We estimated a yield of $2*10^6$ cysts from two pooled T150 culture dishes that were used for one replicate (data not shown). To measure possible metabolite background derived from contaminating host material and magnetic bead preparations, we included uninfected myotubes and bead-supplemented tachyzoites as controls. All preparations were extracted in 80 % acetonitrile and analyzed on a HILIC-UHPLC-LC/MS. The blank and host cell background was subtracted and ion intensities were normalized to the total ion count per sample and log2-fold changes of metabolites between experimental conditions calculated (Fig. S4A-F). Principal component (PC) analysis indicated that bradyzoites

in the purified tissue cysts differed from tachyzoites along PC1, while myotube- and HFF-derived tachyzoites were separated in PC2 (Fig. 5A). Bead-supplemented tachyzoite controls were indistinguishable from pure tachyzoites, and uninfected host cells were similar to bead-only samples, indicating minimal metabolite contamination due to the purification procedures (Fig. S4E). We quantified the levels of 71 metabolites, excluding those that we detected in uninfected controls. The levels of 26 metabolites varied between parasite stages, 10 varied between types of host cells, while 24 depended on both factors, and 11 remained invariant (Fig. 5B-D). Comparing bradyzoites to tachyzoites from the same host cell type (Fig. 5E) we noted that the relative abundances of amino acids and sugar derivatives are generally increased, while vitamins, derivatives of amino acids, nucleic acids and metabolites associated with the TCA cycle are significantly decreased. Fatty acids (FAs) and related molecules are variably affected by stage conversion. When comparing tachyzoites in myotubes with those in HFF-cells (Fig. 5E) we found that the levels of amino acids and sugars were lower in myotube-grown tachyzoites, while FAs increased in abundance. The host cell type had mixed effects on other metabolite classes. Our data reveal distinct metabolic features in *T. gondii* bradyzoites and suggest a downregulation of the mitochondrial TCA cycle in bradyzoites.

**The TCA cycle plays a diminished role in mature *T. gondii* tissue cysts**

To compare the importance of the stage-specific regulation of the TCA cycle between tachyzoites and bradyzoites, we used the aconitase inhibitor sodium fluoroacetate (NaFAc) to inhibit the TCA cycle flux in *T. gondii* (MacRae et al., 2012). Continuous exposure to NaFAc arrests tachyzoite replication with an $IC_{50}$ of 168 µM, and parasite replication was minimal at 500 µM (Fig 6A). We used this concentration to compare the viability of tachyzoites and cysts in the absence of TCA cycle flux. To this end, we exposed 28-day-old cysts and freshly invaded tachyzoites for seven days to NaFac. While tachyzoites did not recover under these conditions, bradyzoites treated with up to 5 mM NaFAc remained viable with an RS of 0.8 (Fig 6B).

These data validate our hypothesis derived from the metabolic data and indicate that the viability of bradyzoites does not rely on a functional TCA cycle.

## Discussion

Persistence mechanisms of important protozoan pathogens, including *T. gondii*, *T. cruzi*, *Leishmania* spp and *P. vivax,* remain largely understudied and there are inadequate or no treatments available against chronic infections with these organisms (Barrett et al., 2019). The limited availability of methods to culture persister cells restricts the approaches to study the link between persistence and metabolism (Barrett et al., 2019; Cerutti et al., 2020). Here, we report a cell culture model based on immortalized human skeletal muscle cells (Shiomi et al., 2011) that supports maturation of tissue cysts of type I, II and III *T. gondii* strains. These myotube-grown bradyzoites exhibit key characteristics including typical ultrastructural features, stress resistance and tolerance towards antimicrobials.

Our *in vitro* system is scalable, enabling global measurements of bradyzoite metabolites via mass spectrometry. To this end, we established a protocol that allows isolation and purification of cysts in large quantities and without the use of percoll gradients (Watts et al., 2015), making them available for mass spectrometry-based metabolomics. We obtained an estimated yield of $2*10^6$ cysts per two T150 culture dishes that were sufficient for one technical replicate and represent a 1,000-fold improvement compared to the yield from the infection of one mouse (Watts et al., 2015). Principal component analysis of the impact of host cell type and the parasite stage indicates mostly independent effects on the metabolome (Fig 5A). Stage conversion leads to changes that are largely homogeneous across classes of metabolites such as amino acids, vitamins, TCA cycle intermediates and nucleic acids. This indicates the operation of distinct metabolic homeostasis mechanisms in bradyzoites.

Bradyzoites harbor lower levels of several TCA cycle-associated metabolites that might reflect lower activity of this pathway (Fig 5E). This is consistent with our results with the aconitase inhibitor sodium fluoroacetate which leads to an accumulation of citric acid and abolishes growth and viability of tachyzoites (MacRae et al., 2012) but does not affect the viability of bradyzoites (Fig 6). Of note, the activity of the TCA cycle enzyme isocitrate dehydrogenase has been detected in lysates of 4-week-old bradyzoites from mice (Denton et al., 1996). Hence, the TCA cycle may represent an active but dispensable source of ATP in this stage. This notion complements previous findings that point towards glycolytic ATP production in bradyzoites. The number of *T. gondii* cysts in brain tissue of latently infected mice depends on the turnover of large amylopectin pools (Sugi et al., 2017) and on the expression of several glycolytic enzymes including hexokinase (Shukla et al., 2018) and lactate dehydrogenase (Abdelbaset et al., 2017;

Xia et al., 2018). Interestingly, transcriptomic analyses of *P. vivax* hypnozoites, a persistent stage of this malaria parasite, indicates a similar metabolic shift towards glycolysis (Bertschi et al., 2018).

We also found that a number of amino acids were accumulated in bradyzoites (Fig 5E). All of these amino acids can be imported by extracellular tachyzoites, indicating the presence of respective Apicomplexan Amino Acid Transporters (ApiATs) (Parker et al., 2019). Except TgApiAT5-2 which is induced in bradyzoites, the transcript expression of these transporters appears only marginally affected by stage conversion (Pittman et al., 2014), suggesting that also bradyzoites have the ability to import required amino acids. The affected amino acids except for proline, which can also be synthesized from glutamate (Krishnan et al., 2020), are less concentrated in the RPMI-based bradyzoite medium compared to the DMEM-based medium used for tachyzoites, implying an endogenous origin of these differences. Hence, these changes may reflect a lowered demand for protein biosynthesis and may also be associated with an additional source. Autophagy and proteolysis through autophagy-related protein (ATG9) (Smith et al., 2020) and cathepsin L (Dou et al., 2014) has been shown to be essential in bradyzoites and may constitute an endogenous source for amino acids. Interestingly, restriction of some exogenous amino acids can be used to facilitate stage conversion (Cerutti et al., 2020; Jeffers et al., 2018). Together, these data support a model in which differentiation to bradyzoites presents a mechanism to cope with limited availability of exogenous amino acids. The diversification of nutrient sources would resemble the stringent metabolic response of *Leishmania mexicana* amastigotes that adopt a slow growing phenotype within the phagolysosome of macrophages (Saunders et al., 2014).

Nucleobase-containing metabolites were found to be less abundant in bradyzoites. While the parasite is auxotroph for purines, pyrimidines can both be imported and synthesized (Fox and Bzik, 2002). Slowly growing or dormant bradyzoites likely require lower amounts of nucleobases. Consistently, the transcription of the corresponding low affinity and high-capacity adenosine transporter TgAT (Chiang et al., 1999; De Koning et al., 2003) appears to be down-regulated in 4-week-old bradyzoites *in vivo* (Fig S5). Two other proteins containing nucleoside transport signatures remain expressed and may represent the unidentified high affinity purine transporter being responsible for maintaining a slow influx of nucleobases (Fig S5) (Pittman et al., 2014). Pyrimidine salvage does not appear to be essential for bradyzoite formation (Fox et al., 2011) indicated by its continued synthesis. Similar to *P. falciparum* (Painter et al., 2007), pyrimidine synthesis in *T. gondii* depends on the mitochondrial electron transport chain (mETC)

to provide an electron acceptor, dihydroorotate dehydrogenase (Hortua Triana et al., 2012). While we show that *in vitro* bradyzoites develop tolerance towards the bc1-complex inhibitor HDQ (Hegewald et al., 2013) other inhibitors of this complex, including quinolones and atovaquone, lead to a decrease in cyst counts but not their clearance in brains of latently infected mice (Araujo et al., 1991; Doggett et al., 2012; Ferguson et al., 1994b). The cytotoxicity of atovaquone against KD3 myotubes (data not shown) prevented us from assessing its activity against *in vitro* tissue cysts. Together, available data suggests that the bc1-complex is a viable target in tissue cysts and the tolerance towards HDQ might reflect its pharmacological properties. In the absence of an obligate TCA cycle an indispensable function of the mETC in bradyzoites likely includes pyrimidine synthesis.

*T. gondii* is a remarkably promiscuous pathogen, and the ability to infect disparate host cell types demands metabolic flexibility. We found that the metabolome of *T. gondii* indeed depends on the host cell type, although the influence of stage conversion appears much larger (Fig 5A, B). Notably, the levels of the three essential amino acids methionine, threonine and phenylalanine were decreased in myotube-grown tachyzoites compared to HFF-grown tachyzoites. These lowered levels may reflect a lower abundance of these amino acids in myotubes. Essential amino acids including phenylalanine and tryptophan were reported to be decreased during myotube differentiation of primary human skeletal muscle cells (Kumar et al., 2020). Similar metabolic changes are caused by induction of the FOXO1 transcription factor (Matsuda et al., 2019) that is typically induced in skeletal muscle cells (Gross et al., 2008). Limited supply of these amino acids may facilitate stage conversion in myotubes through slowing down tachyzoite growth (Cerutti et al., 2020; Jeffers et al., 2018).

Multinucleated myotubes are generally arrested in the G0 phase of the cell cycle and exhibit highly branched mitochondria and oxidative metabolism as opposed to glycolytic lactate production (Malinska et al., 2012). Both traits have been shown to also facilitate stage conversion of *T. gondii* (Radke et al., 2006; Swierzy and Lüder, 2015; Weilhammer et al., 2012) and may contribute to the suitability of KD3 cells to harbor *T. gondii* tissue cysts by limiting the expansion of non-converting tachyzoites. While the differentiation efficiency of all tested *T. gondii* strains can be further increased by additional non-physiological stressors such as basic pH it is not needed for extended cultures. Strikingly, even highly virulent RH-derived parasite sub-strains did not overgrow the culture (Fig 2C). Resistance of bradyzoites against pepsin digestion and temperature stress develops after 14 days post infection and increases until 28 days post infection (Fig 3C). The onset of tolerance towards inhibitors of well-established drug targets including the

calcium-dependent protein kinase 1 (TgCDPK1) (Scheele et al., 2018; Winzer et al., 2015), dihydrofolate reductase-thymidylate synthase (TgDHFR-TS) (Roos, 1993) and the mitochondrial bc1-complex follows similar timing and is shared with *T. gondii* cysts in the brain of chronically infected mice (Bajohr et al., 2010; Saleh et al., 2007; Scheele et al., 2018; Winzer et al., 2015). Hence, our *in vitro* model will facilitate dissecting the molecular basis of the impressive drug tolerance and stress resistance of *T. gondii* tissue cysts.

Electron microscopic analysis of the ultrastructure of myotube-derived tissue cysts revealed typical features such as a developing cyst wall, amylopectin granules and posterior positioned nuclei in the bradyzoites (Fig 2A, S1) (Ferguson et al., 1994a). Interestingly, we also found evidence of disintegrating bradyzoites at all time points (up to 21 days post infection, (Fig S1) that has also been described previously in mice after four and eight weeks of infection (Ferguson et al., 1994a; Watts et al., 2015; Yap et al., 1998). This parasite turnover likely contributes to the heterogeneous appearance with respect to cyst size and bradyzoite packaging density (Ferguson and Hutchison, 1987; Watts et al., 2015). A similar phenotypic heterogeneity has been ascribed to the ability of other intracellular pathogens to persist in the presence of stressors such as drugs and immune effectors (Bakkeren et al., 2020).

In conclusion, we present a novel system to culture functionally mature *T. gondii* tissue cysts that surpasses typical *in vivo* systems in yield by several orders of magnitude and allows their purification with methods compatible with subsequent mass spectrometry-based metabolomics. The bradyzoite metabolome emphasizes the importance of amino acids while the TCA cycle is active but dispensable.

**Acknowledgements / Funding**

We are grateful to Naohiro Hashimoto for sharing KD3 skeletal muscle cells, David Siblely for sharing DG52 antibodies, Wesley Van Voorhis and Wolfgang Bohne for sharing BKIs and HDQ, respectively; Alexander Neumann for sharing CCEAN software; Gereon Schares, Marie-France Cesbron-Delauw, Jonathan Howard, Boris Striepen for *T. gondii* strains and Anton Aebischer and Dominique Soldati-Favre for helpful discussions. MB, CC, DM, JS, FM are funded by the Federal Ministry of Education and Research (BMBF) under project number 01KI1715 as part of the “Research Network Zoonotic Infectious Diseases”. FS is a senior member of graduate schools GRK 2046 and IRTG 2290, supported by the German Research Council (DFG). TS receives support from the Deutsche Forschungsgemeinschaft (DFG) (STE 2348/2), MML is funded (Research Grants-Doctoral Programmes in Germany) by the German Academic Exchange Service (DAAD). MB, CC, DM, JS, FM, TH and FS receive internal support from the Robert Koch-Institute.

**Author Contributions**

Conceptualization, M.B.; Methodology, M.B., F.S., C.C., D.M.; Investigation: C.C., J.S., D.M., F.M., T.H., M.M.L.; Writing –Original Draft: M.B. and C.C.; Writing –Review & Editing: all authors; Funding Acquisition, M.B.; Supervision, M.B.

**Declaration of Interests**

The authors declare no competing interests.

**Main Figure Legends**

**Figure 1: KD3 human myoblasts form multinucleated myotubes.** (A) Immunofluorescence images of KD3 myoblasts and myotubes after five days of differentiation stained for myosin heavy chain (MF20) and DNA (DAPI). (B) As a morphological parameter of myotube formation, the myogenic index (fraction of nuclei in a multinucleated cell) was measured in at least 10 different randomly selected locations by CCEAN software (Neumann, 2014). Values are expressed as mean ± SEM of two individual experiments performed in triplicates (***p<0.001, Mann-Whitney-U-test).

**Figure 2: Time- and pH-dependent cyst maturation of type I, II and III *T. gondii* strains in KD3 myotubes.** (A.) Electron microscopy of 7-, 14- and 21-day-old Pru-tdTomato tissue cysts in KD3 myotubes (days post-infection; d.p.i.). Cysts show a distinct wall (CW) and are densely packed with parasites containing amylopectin granules (A) and nuclei (N). (B) Immunofluorescence imaging of KD3 myotubes infected with type I (RH, RHΔ*ku80*, GT1), type II (ME49, NTE, Pru-tdTomato) and type III (NED, VEG) parasites. Cyst formation was induced for 7, 14 and 21 days under neutral or basic pH and stained with anti-CC2, anti-SAG1 antibodies and DBA. Shown are representative images of tachyzoite controls infected with RHΔ*ku80* for 24 h (upper panel), 14-day-old intermediate cysts (middle panel) and mature cysts (lower panel) of the NED strain. Scale bar indicates 5 µm (C.) Relative numbers of SAG1-negative but DBA and CC2-positive cysts counted from three independent blinded experiments performed in triplicates. At least 25 DBA positive cysts per strain, time point and replicate were counted. Values represent means ± SEM.

**Figure 3: *In vitro* bradyzoites develop resistance to pepsin, tolerance to temperature stresses and are orally infectious to mice.** (A.) Experimental design of *in vitro* pepsin and oral transmission assay. Pru-tdTomato cysts and tachyzoite controls were challenged with indicated pepsin and/or temperature stresses. Treated parasites were seeded onto fresh human fibroblasts to induce tachyzoite re-differentiation and proliferation. tdTomato fluorescence was monitored in a fluorescent based plate reader. (B.) Raw fluorescence intensities of 21-day-old cysts digested for 20 (red), 40 (blue) and 60 min (green) and the respective tachyzoite control (grey). Dashed lines indicate corresponding untreated controls. The black dotted line indicates the limit of detection. The data represent the means and SEM of one experiment consisting of three digestion reactions (C.) Resistance scores of tachyzoite cultures (0), 14-, 21- and 28-day-old cysts after 20 (red), 40 (blue), 60 min (green) of pepsin digestion. Shown are the means and SEM of three independent experiments performed in triplicates (*p≤0.05, Mann-Whitney-U-test). (D.)

Resistance scores of 35-day-old bradyzoites exposed to indicated temperature stresses and pepsin digestion. Values are expressed as means and SEM from three or two independent experiments in triplicates (**p<0.005, ***p<0.001, Mann-Whitney-U-test). (E.-F.) Seroconversion and weight loss of mice that were orally infected with 50 or 500 35-day-old Pru-tdTomato cysts. Each group consisted of five mice. (E.) Seroconversion was checked for *T. gondii* specific IgGs via ELISA. Each data point represents the mean and SEM of absorbance (450 nm - 570 nm) in duplicates from serum of a single mouse (**p≤0.05, Mann-Whitney-U-test). (F.) The weight was monitored over a time period of 30 days. Each point represents the means of one experiment consisting of five infected animals per group with ± SEM (*p<0.005, Mann-Whitney-U-test).

**Figure 4: *T. gondii in vitro* bradyzoites develop broad drug tolerance.** (A.) Experimental design for *in vitro* drug tolerance assay. Pru-tdTomato cysts and tachyzoite controls were drug treated at the indicated concentrations for one week. Following the treatment, medium was changed to bicarbonate-replete medium to induce re-differentiation to proliferating tachyzoites and tdTomato fluorescence was monitored. (B.) Raw fluorescence intensities of a representative experiment during cyst maturation for 14 days, 7 days of treatment with 20 µM pyrimethamine or 0.2 % DMSO as solvent control and re-differentiation for 28 days. Black dotted line indicates the limit of detection. Data represents the means and SEM of one experiment with five replicates. (C.-D.) Resistance scores of tachyzoites (0) and 14-, 21- and 28-day-old bradyzoites treated with pyrimethamine (PYR), sulfadiazine (SULF) or 1-hydroxy-2-dodecyl-4(1*H*) quinolone (HDQ) and bumped kinase inhibitor (BKI) 1553 and BKI 1294. Shown are means of three independent experiments with five replicates each and SEM (*p≤0.05, Mann-Whitney-U-test).

**Figure 5: *T. gondii in vitro* tissue cysts harbor a distinct metabolome** (A.) Principal component analysis of untargeted metabolomic data comparing 28-day-old ME49 *T. gondii in vitro* cysts cultivated in KD3 myotubes, tachyzoites in KD3 myotubes and tachyzoites (Tz) in HFFs. Two individual experiments with four replicates each were analyzed. (B.) Pie chart showing the number of metabolites within the dataset and how they were affected by host cell environment and parasite stage. (C.-D.) Volcano plots of log2-fold changes calculated from fractional metabolite abundances between *in vitro* cysts and myotube-isolated tachyzoites or (D.) tachyzoites isolated from and HFFs (n=8, Mann-Whitney-U-test). (E.) Heatmap showing log2-fold changes of significantly different metabolites ($p < 0.05$, uncorrected Mann-Whitney-U test) between *in vitro* cysts and tachyzoites in myotubes (left panel) and tachyzoites in myotubes compared to tachyzoites in HFFs (right panel). Log2-fold changes were calculated pair-wise. Grey areas indicate non-significantly changed metabolites. Asterisks denote putative metabolite identifications based on accurate mass only. AcGlutamate: acetylglutamate, AcCarnitine: acetylcarnitine, UDP-NAc-GlcN: UDP-N-acetyl-glucosamine, GABA: γ-aminobutyric acid, GroPIns: glycerphosphoinositol, GroPEtn: glycerophosphoethanolamine, G3P: glycero-3-phosphate.

**Figure 6: Tachyzoites but not bradyzoites require a functional TCA cycle for viability.** (A.) Calculation of inhibitory concentrations ($IC_{50}$) of sodium fluoroacetate (NaFac) for Pru-tdTomato tachyzoites. Parasites were grown for seven days in presence of NaFac and the $IC_{50}$ value was calculated from fluorescence intensities normalized to untreated controls. Shown are means and SEM of three independent experiments with three replicates each. (B.) Resistance scores of

tachyzoites and 28-day-old bradyzoites treated with NaFac or 0.5 % water as solvent control. Shown are means and SEM of two and three independent experiments for bradyzoites and tachyzoites performed in triplicates, respectively (*p≤0.05, Mann-Whitney-U-test).

## Materials and Methods

### Host cell lines and cultivation

All cultures were maintained in a 37 °C humidified $CO_2$ (10 %) incubator as described previously (Blume et al., 2015).

Briefly, human foreskin fibroblast (HFF) monolayers were cultured in Dulbecco's Modified Eagle's Medium (DMEM) (Gibco) supplemented with 25 mM glucose (Sigma-Aldrich), 4 mM L-glutamine (Thermo Fisher Scientific), 1 mM sodium pyruvate (Capricorn Scientific), 100 U/ml penicillin, 100 µg/ml streptomycin (Thermo Fisher Scientific) and 10 % heat-inactivated calf serum (Capricorn Scientific).

The immortalized human myoblast cell line KD3 (a kind gift of N. Hashimoto; (Shiomi et al., 2011)), initially derived from normal subcutaneous female muscle tissue, was cultured in DMEM supplemented with 25 mM glucose, 4 mM L-glutamine, 1 mM sodium pyruvate, 100 U/ml penicillin, 100 µg/ml streptomycin, 2 % Ultroser G (Cytogen GmbH) and 20 % heat inactivated fetal bovine serum (FBS). The differentiation of myoblasts into myotubes was induced at 70 % confluency by changing medium to DMEM supplemented with 25 mM glucose, 4 mM L-glutamine, 1 mM sodium pyruvate, 100 U/ml penicillin, 100 µg/ml streptomycin, 2 % horse serum (HOS) (Capricorn Scientific), 10 µg/ml human insulin (Sigma-Aldrich), 5 µg/ml human holo-transferrin (PAN Biotech) and 1.7 ng/µl sodium selenite (Sigma-Aldrich) for five to seven days (Shiomi et al., 2011).

### Parasite strains cultivation and differentiation

Type I strain RH (Sabin, 1941), RH-*Δku80Δhxgprt* (RH*Δku80*) (Huynh and Carruthers, 2009), GT1 (Dubey, 1980), Type II ME49 (Guo et al., 1997), NTE (Guo et al., 1997), Pru-*Δku80Δhxgprt(BSG-4) (*Pru-GFP*)* (Singh et al., 2002), Pru-*Δhxgprt* tdTomato (Pru-tdTomato) (John et al., 2009) and Type III NED (Darde et al., 1992), VEG (provided by G. Schares, (Sibley et al., 2002)) were maintained *in vitro* in HFF monolayers grown in DMEM supplemented with 25 mM glucose, 4 mM L-glutamine, 1 mM sodium pyruvate, 100 U/ml penicillin, 100 µg/ml streptomycin and 1 % heat-inactivated FBS (tachyzoite medium). Freshly egressed parasites were passaged by transfer to new HFF monolayers. Differentiation of tachyzoites into tissue cysts was facilitated by $CO_2$ depletion at pH 7.4 if not otherwise indicated. To avoid acidification, the medium was changed to low glucose (5 mM), 50 mM HEPES (Sigma-Aldrich) buffered Roswell

Park Memorial Institute 1640 (RPMI) medium (Gibco) supplemented with 4 mM L-glutamine, 100 U/ml penicillin, 100 µg/ml streptomycin, 2 % HOS and ITS (bradyzoite medium). The cells were incubated at 37 °C and ambient $CO_2$ levels. Medium was changed every second day. For assays involving plate reader-based fluorescence measurements, phenol red was omitted from the medium.

**Electron microscopy**

KD3 myotube cultures in T60 dishes were infected with Pru-tdTomato tachyzoites at a multiplicity of infection (MOI) of 0.3, and bradyzoite formation was facilitated for the indicated times in bradyzoite medium at ambient $CO_2$ levels. On the day of the experiment the medium was removed and samples were fixed by covering the monolayer with 1 % paraformaldehyde (Sigma-Aldrich) and 2.5 % glutaraldehyde (Sigma-Aldrich) in 0.05 M HEPES buffer (pH 7.4). After incubation at RT for 3 h, samples were sealed with parafilm and stored in the fridge until further processing.

For plastic embedding cells were scraped off with a cell scraper, sedimented by centrifugation (3000 x *g*, 10 min) and washed twice with 0.05 M HEPES buffer for removing the fixative. The washed cell pellets were mixed with 3 % low-melting point agarose (1:1 [v/v]) at 40 °C, centrifuged (3000 x *g*,5 min) and cooled on ice. The cell pellets were cut off from the agarose gel block using a sharp razor blade and stored in 2.5 % glutaraldehyde in 0.05 M HEPES buffer. Post-fixation, block contrasting and dehydration, embedding in epoxy resin was performed according to a standard procedure (Laue, 2010). Ultrathin sections with a thickness of ~65 nm were generated with an ultramicrotome (UC7, Leica Microsystems, Germany) using a diamond knife (45°, Diatome, Switzerland), collected on copper slot grids and contrasted with 2 % uranyl acetate and 0.1 % lead citrate.

Electron microscopy of ultrathin sections was performed with a transmission electron microscope (Tecnai Spirit, Thermo Fisher Scientific) at 120 kV. Images were recorded with a side-mounted CCD camera (Megaview III, EMSIS, Germany) and the montage function of the camera software (Multiple Image Alignment, iTEM; EMSIS, Germany) was used to cover larger field of views with sufficient pixel resolution.

**Immunofluorescence assay**

Uninfected host cells were grown in monolayers on 12 mm round glass coverslips and infected for 24 h unless indicated otherwise. Samples were fixed with 4 % paraformaldehyde in phosphate buffered saline (PBS) (Thermo Fisher Scientific) for 20 min at RT followed by a washing step in 0.1 M glycine/PBS (Thermo Fisher Scientific) and permeabilization for 20 min in 0.1 M Triton X-100 (Thermo Fisher Scientific) in PBS. Cells were blocked for 1 h in 2 % bovine serum albumin (BSA) (Thermo Fisher Scientific) in PBS, stained for 1.5 h with primary and for 1 h with species-matched secondary antibodies at RT and mounted on microscopy slides (Thermo Fisher Scientific) in Fluoromount-G (Sigma-Aldrich) containing DAPI (1:3,000) (Thermo Fisher Scientific). Samples were first stained with biotinylated *Dolichos biflorus* agglutinin (DBA) 1:1,000 (Sigma-Aldrich) and primary monoclonal antibodies (mAb) (anti-rat CC2 1:1,000 (Gross et al., 1995); anti-mouse myosin heavy chain (MF20) 1:400 (eBioscience™); anti-mouse surface antigen 1 (SAG1) mab DG52 1:500 (Bulow and Boothroyd, 1991)) and then for 1 h with goat anti-rat-Alexa546 1:300 (Invitrogen), goat anti-rat-Alexa375 1:300 (Thermo Fisher Scientific), rabbit anti-mouse-Cy3 1:400 (Dianova), donkey anti-mouse-Cy5 1:300 (Dianova) or streptavidin-Alexa488 1:2,500 (Invitrogen), and streptavidin-Cy5 1:2,500 (Jackson antibodies). Monochromatic images were recorded on a Zeiss Apotome Imager equipped with a Plan-Fluar" 63x/1.45 oil M27 objective and imported into ImageJ (Schneider et al., 2012) for coloring and the generation of overlays.

**Pepsin digestion and *in vitro* oral transmission assay**

KD3 myotube cultures in 6-well plates were infected with Pru-tdTomato tachyzoites at an MOI of 0.1 and bradyzoite formation was induced for the indicated times in bradyzoite medium. Tachyzoite controls were infected for two days at MOI of 5 in tachyzoite medium. On the day of experiment, pepsin digestion was performed for 20, 40 and 60 min at 37 °C as described previously (Dubey, 1998) using a modified pepsin solution. The buffered solution consisted of 1.01 g pepsin (Thermo Fisher Scientific), 0.166 g glycine (Thermo Fisher Scientific), 0.129 g NaCl (Sigma-Aldrich) and 17.8 ml of a 1M HCl solution (Sigma-Aldrich), filled up to 200 ml with Milli-Q-water, resulting in a pH of 1.2 and supplemented with 5 mM glucose. Digestion was terminated by neutralization using a 1.2 % sodium bicarbonate solution (pH≈8.3) containing 0.0159 g/l phenol red as pH indicator dye. Digested infected monolayers and uninfected and undigested controls were collected with a cell scraper and harvested via centrifugation (1,200 x *g*, 10 min). The supernatant was then removed, the pellets were resuspended in 450 µl DMEM tachyzoite medium

and used to infect HFF cells in a 96-well plate in triplicates for pepsin digests (Fig 3C) transmission assays (Fig 3D). Parasite recovery was monitored by measuring tdTomato fluorescence intensity (excitation 554 nm / emission 589 nm) in a plate reader (Tecan Infinite M200 PRO) every second day for up to 21 days. Medium was exchanged after each measurement.

For the oral transmission assay scraped monolayers and controls were challenged by the indicated combination of stresses: cold stress (4 °C for four and seven days), heat stress (55 °C or 65 °C for 5 min), incubation at RT for two days, and pepsin digestion (60 min).

The resistance score (RS) was calculated from the number of days passed until detection of tachyzoite growth by fluorescence intensity of Pru-tdTomato parasites:

$$RS = 1 - (\#days_{treatment} - \#days_{vehicle}) / \#days_{observed}$$

An RS of 0 indicates no recovery from the treatment and a RS of 1 means equal growth to the untreated control, indicating full resistance to the treatment.

### *In vivo* oral transmission assay

KD3 myotube cultures in 6-well plates were infected with Pru-tdTomato tachyzoites at an MOI of 0.3. Bradyzoite formation was induced for indicated time in bradyzoite medium. The cyst cultures were then prepared for shipping and sent to Freiburg at RT within 24 h. The cysts were washed once with PBS, scraped in fresh bradyzoite medium and harvested via centrifugation (1,200 x *g*, 10 min). The supernatant was removed after centrifugation and the pellet was resuspended in 2 ml PBS and placed on ice. For quantification, 10 µl of the cyst solution was placed on a glass slide and intact cysts were counted based on the fluorescence of tdTomato in a fluorescence microscope.

### Mouse infections

Groups of five 10-week-old male mice (C57BL/6JRj) were obtained from certified breeders (Janvier Labs, Route du Genest, 53940 Le Genest-Saint-Isle, France) and kept under specific-pathogen-free conditions in the local animal facility (Department for Microbiology and Hygiene, Freiburg). All animal experiments were performed in accordance with the guidelines of the German animal protection law and the Federation for Laboratory Animal Science Associations. Experiments were approved by the state of Baden-Württemberg (Regierungspräsidium Freiburg; reference number 35-9185.81/G-19/89).

Mice were infected by oral gavage with 50 or 500 freshly prepared *in vitro*-generated Pru-tdTomato cysts in a total volume of 200 µl PBS. Infected mice were monitored and weighed daily for the duration of the experiment. After 30 days post infection blood samples from all mice were collected from the facial vein. Blood was allowed to clot at RT for 30 min before centrifugation at (500 g, 10 min). Serum was collected and either immediately analyzed, or stored at -20 °C. Animals were euthanized by cervical dislocation. Brains were harvested in 2 ml PBS and minced using an 18 G needle for cysts inspection via DBA staining as described previously (Matta et al., 2019).

Seroconversion was evaluated via ELISA as described previously (Matta et al., 2019). Serum from non-infected (n.i) mice were included to calculate the cutoff:

cutoff = mean $Absorbance^{450nm-570nm}$ (n.i.) + 2 x standard deviation of $Absorbance^{450nm-570nm}$ (n.i.)

Values higher than the cut off were considered as positive.

**Cyst isolation**

Two T150 dishes per sample were infected with Pru-tdTomato tachyzoites at an MOI 0.3 and cyst formation was induced for indicated time. On the day of harvest, dishes were placed on ice, medium was removed and infected and uninfected monolayers were washed three times with ice-cold PBS. Cells were then harvested by scraping into 10 ml ice-cold 0.05 % BSA in PBS per T150 dish. Cysts were released from the monolayer via forcing through a 23G needle (Sterican®) 25 times with a syringe and collected via centrifugation (1,200 x *g*, 10 min, 0 °C). The supernatant was removed, the pellet was resuspended carefully in 2 % BSA in PBS containing 7 x $10^8$ DBA-coupled beads (preparation described below) and samples were incubated for 1 h at 4 °C with gentle shaking. Subsequently, the samples were placed in a magnetic stand on ice, washed five times with 0.1 % BSA in PBS to remove cell debris, followed by two washing steps with PBS to remove residual BSA. Cysts and beads were then collected via centrifugation (1,200 x *g*, 10 min, 0 °C), shock frozen in liquid nitrogen and stored at -80 °C until extraction. All samples were extracted simultaneously in 80 % acetonitrile for LC/MS analysis as described below. Uninfected controls and bead-only controls were processed equally.

**Preparation of beads**

Coupling of Dynabeads™ MyONE™ Streptavdin T1 (Thermo Fisher Scientific) to DBA was done as described in the manufacturer's protocol. Briefly, 7 x $10^8$ beads were resuspended in 1 ml PBS

by vortexing, washed three times with PBS in a magnetic stand and resuspended in 1 ml PBS containing 10 µg DBA / sample. The tube containing the DBA-magnetic bead mixture was incubated on a rotary mixer for 45 min at RT. Uncoupled DBA was removed by washing the coated beads three times with PBS. After washing, the DBA-coated beads were resuspended in 2 ml PBS containing 2 % BSA.

**Untargeted metabolic analysis of *in vitro* cysts**

For metabolome measurements of tissue cysts, cyst maturation and isolation were performed as described above. Metabolites were extracted in 80 % acetonitrile (Carl Roth) and 20 % water (Carl Roth) containing internal standards (phenolphthalein, CAPS, PIPES (Sigma-Aldrich)). Cell pellets were sonicated for 5 min and after centrifugation (21,500 x *g*, 5 min, 0 °C), the supernatants were transferred to MS vials for immediate LC/MS analysis. 5 µL of each sample were collected to generate a pooled biological quality control (PBQC). 20 µL of the *in vitro* cysts, bead control and host cell background samples, and 5 µL of the tachyzoite samples were injected. The injection order of the samples was randomized, blanks and PBQCs were injected periodically. The samples were analyzed on a Q-Exactive Plus mass spectrometer (Thermo Fisher Scientific) via 70k MS1 scans, with intermittent 35k data-dependent 35k MS2 scans in positive and negative mode separately.

Chromatographic separation was achieved on a Vanquish Flex fitted with an ACQUITY UPLC BEH Amide column (Waters). Running a 25 min linear gradient starting with 90 % eluent A (10 mM ammonium carbonate in acetonitrile) / 10 % eluent B (10 mM ammonium carbonate in water) and ending with 40 % eluent A / 60 % eluent B, followed by washing and equilibration steps.

Compound Discoverer 3.1 software (Thermo Fisher Scientific) was used for peak detection, combination of adducts and compound annotation. Metabolite identifications were based on either retention time and accurate mass match to an inhouse library of 160 authentic standards, or by matching accurate mass and MS2 fragments to m/z cloud database (Thermo Fisher Scientific). Data were exported to Excel for grouping, combination of datasets from positive and negative ionization runs and blank subtraction. Compounds with a coverage less than 50 % in at least one sample group were excluded. All missing values were gap filled with either the respective mean of each sample group or the global minimum intensity when undetected in a sample group. After normalization to the internal standard the fractional abundances for each sample were calculated and centered between 1 and -1.

Raw data are deposited at Metabolights database and can be accessed here: www.ebi.ac.uk/metabolights/MTBLS2375 (Haug et al., 2020).

**Drug tolerance assays**

Myotubes in 96-well plates were infected with *T. gondii* Pru-tdTomato tachyzoites at an MOI of 0.1 and cyst formation was induced for indicated times in bradyzoite medium at ambient $CO_2$ levels, followed by a drug pulse of seven days and with respective vehicle as solvent control. Tachyzoite controls were infected with Pru-tdTomato tachyzoites at an MOI of 1 in tachyzoite medium for 2 h before the seven-day drug pulse was applied in tachyzoite medium. Parasite recovery was monitored by measuring tdTomato fluorescence for 28 days as described above. Medium was exchanged after each measurement. The resistance score was calculated as described above for pepsin digestion and the oral transmission assay.

**(i) Developing drug tolerance.** Cysts were generated for indicated times and treated with established antiparasitics (pyrimethamine, sulfadiazine (Sigma)) and HDQ (a kind gift of Wolfgang Bohne), two bumped kinase inhibitors (BKI1294, BKI1553) (Doggett et al., 2014; Huang et al., 2015) or 0.2 % DMSO (Thermo Fisher Scientific) as solvent control at the indicated concentrations for seven days. Respective tachyzoite controls were generated by infecting KD3 myotubes for 2 h at MOI 1 in tachyzoite medium before treatment.

**(ii) Drug resistance of matured cysts vs tachyzoites.** Cyst formation was induced for indicated time and pulsed for seven days with indicated concentrations of sodium fluoroacetate (abcr GmbH) or 0. 5 % $H_2O$ as solvent control. Respective tachyzoite controls were generated as described above.

**(iii) $IC_{50}$ assay tachyzoites.** Growth of tachyzoite controls treated with the indicated concentrations of sodium fluoroacetate was monitored throughout the seven-day drug pulse. The half inhibitory concentration ($IC_{50}$) values were determined at day seven by fitting the dose response curve by non-linear regression in GraphPad Prism v8.

**Statistical analysis**

All tests, except statistics of metabolite abundances were performed in GraphPad Prism v8 as detailed in the results section. Statistical significance of metabolite changes was calculated in Microsoft Excel. Principal component analyses were computed using ClustVis (Metsalu and Vilo, 2015).

## Supplemental Information

**Video S1: Spontaneous contraction of differentiated KD3 human myotubes.** Short video sequences were recorded on a Zeiss Observer equipped with a 63X oil immersion objective

**Figure S1: Micrographs of maturing Pru-tdTomato in KD3 human myotubes.** Electron microscopy of (A.) 7-, (B.) 14- and (C.) 21 day- old Pru-tdTomato tissue cysts matured in KD3 myotubes as shown in Fig 2 (post-infection; p.i.). Images of a single section plane through entire cysts were taken for each time point. Each overview image (upper left) is grouped with three images showing enlarged areas, such as individual parasites with their nuclei (N), amylopectin granules (A) or the cyst wall (CW). In the example shown here, the cyst wall is already well developed 7 days post infection. Other cysts at this time point reveal an immature cyst wall, which is shown in the left image of the additional image panel on the lower right side (D.). At this stage the parasitophorous vacuolar membrane (PVM) is associated with a loose matrix containing vesicles and membrane-bound tubules. In cysts 21 post induction (shown at the right side of this image panel), the cyst wall (CW) is formed by a dense and rather homogenous matrix which is associated with the PVM.

**Figure S2: Influence of different host cell environments on spontaneous cystogenesis of *T. gondii*.** Human KD3 myoblasts, myotubes and fibroblasts were infected with *T. gondii* Pru-GFP (MOI: 3) that express GFP under the bradyzoite-specific LDH2-promoter. Monolayers are stained for DNA (DAPI). The GFP signal indicates spontaneous stage conversion to early bradyzoite stages after 72 post-infection in bicarbonate-replete conditions.

**Figure S3: *T. gondii* tissue cysts isolated from brains of chronically infected mice that were inoculated with *in vitro* Pru-tdTomato cysts.** Immunofluorescence microscopy of a cyst, isolated from the brain of a mouse orally infected with Pru-tdTomato *in vitro* cysts, stained with DBA-FITC. DBA: *Dolichos biflorus* agglutinin. Scale bar indicates 10 µm.

**Figure S4: Data curation LC/MS.** Samples were analyzed in positive and negative ionization mode separately. The principal component analyses illustrate effects of the data analysis steps. (A.) Positive and negative datasets were combined. (B.) Blanks were subtracted. Metabolites that had a coverage of less than 50 % in at least one sample set were excluded. (C.) Gaps in the dataset were filled with the mean intensity of the sample group of the respective batch. If a metabolite was not detected in sample group the minimal intensity value was used for gap filling. (D.) Metabolites that were prominent within the magnetic bead or host cell background samples were excluded. (E.) To allow statistical comparison of the cyst samples, which were not normalized to parasite numbers, with the tachyzoites samples, the fractional abundances were calculated by dividing each metabolite intensity by the sum of all intensities per sample. (F.) Since the bead background within the tachyzoite samples did not play an important role, they were excluded.

**Figure S5: Transcriptomic data of amino acid transporter genes of *T. gondii* from Pittman et al., 2014.**

Transcripts per kilobase million were downloaded from ToxoDB (http://www.toxodb.org) and analyzed for stage specific regulation by dividing expression values for acute (10 days post infection (d.p.i.)) by chronic infection in mice (28 d.p.i.).

## References

Abdelbaset, A.E., Fox, B.A., Karram, M.H., Abd Ellah, M.R., Bzik, D.J., and Igarashi, M. (2017). Lactate dehydrogenase in Toxoplasma gondii controls virulence, bradyzoite differentiation, and chronic infection. PLoS One 12, e0173745.

Araujo, F.G., Huskinson, J., and Remington, J.S. (1991). Remarkable in vitro and in vivo activities of the hydroxynaphthoquinone 566C80 against tachyzoites and tissue cysts of Toxoplasma gondii. Antimicrob Agents Chemother 35, 293-299.

Bajohr, L.L., Ma, L., Platte, C., Liesenfeld, O., Tietze, L.F., Gross, U., and Bohne, W. (2010). In vitro and in vivo activities of 1-hydroxy-2-alkyl-4(1H)quinolone derivatives against Toxoplasma gondii. Antimicrob Agents Chemother 54, 517-521.

Bakkeren, E., Diard, M., and Hardt, W.-D. (2020). Evolutionary causes and consequences of bacterial antibiotic persistence. Nat. Rev. Microbiol. 18, 479-490.

Barrett, M.P., Kyle, D.E., Sibley, L.D., Radke, J.B., and Tarleton, R.L. (2019). Protozoan persister-like cells and drug treatment failure. Nat. Rev. Microbiol. 17, 607-620.

Bertschi, N.L., Voorberg-van der Wel, A., Zeeman, A.M., Schuierer, S., Nigsch, F., Carbone, W., Knehr, J., Gupta, D.K., Hofman, S.O., van der Werff, N., et al. (2018). Transcriptomic analysis reveals reduced transcriptional activity in the malaria parasite Plasmodium cynomolgi during progression into dormancy. Elife 7.

Blume, M., Nitzsche, R., Sternberg, U., Gerlic, M., Masters, S.L., Gupta, N., and McConville, M.J. (2015). A Toxoplasma gondii Gluconeogenic Enzyme Contributes to Robust Central Carbon Metabolism and Is Essential for Replication and Virulence. Cell Host Microbe 18, 210-220.

Blume, M., and Seeber, F. (2018). Metabolic interactions between Toxoplasma gondii and its host. F1000Res. 7.

Bulow, R., and Boothroyd, J.C. (1991). Protection of mice from fatal Toxoplasma gondii infection by immunization with p30 antigen in liposomes. J. Immunol. 147, 3496-3500.

Cerutti, A., Blanchard, N., and Besteiro, S. (2020). The Bradyzoite: A Key Developmental Stage for the Persistence and Pathogenesis of Toxoplasmosis. Pathogens 9.

Chiang, C.W., Carter, N., Sullivan, W.J., Jr., Donald, R.G., Roos, D.S., Naguib, F.N., el Kouni, M.H., Ullman, B., and Wilson, C.M. (1999). The adenosine transporter of Toxoplasma gondii. Identification by insertional mutagenesis, cloning, and recombinant expression. J. Biol. Chem. 274, 35255-35261.

Darde, M.L., Bouteille, B., and Pestre-Alexandre, M. (1992). Isoenzyme analysis of 35 Toxoplasma gondii isolates and the biological and epidemiological implications. I. J. for Parasitol. 78, 786-794.

De Koning, H.P., Al-Salabi, M.I., Cohen, A.M., Coombs, G.H., and Wastling, J.M. (2003). Identification and characterisation of high affinity nucleoside and nucleobase transporters in Toxoplasma gondii. I. J. for Parasitol. 33, 821-831.

Denton, H., Roberts, C.W., Alexander, J., Thong, K.W., and Coombs, G.H. (1996). Enzymes of energy metabolism in the bradyzoites and tachyzoites of Toxoplasma gondii. FEMS microbiology letters 137, 103-108.

Desmonts, G., Couvreur, J., Alison, F., Baudelot, J., Gerbeaux, J., and Lelong, M. (1965). [Epidemiological study on toxoplasmosis: the influence of cooking slaughter-animal meat on the incidence of human infection]. Rev. Fr. Etud. Clin. Biol. 10, 952-958.

Di Cristina, M., Dou, Z., Lunghi, M., Kannan, G., Huynh, M.H., McGovern, O.L., Schultz, T.L., Schultz, A.J., Miller, A.J., Hayes, B.M., et al. (2017). Toxoplasma depends on lysosomal consumption of autophagosomes for persistent infection. Nat. microbiology 2, 17096.

Doggett, J.S., Nilsen, A., Forquer, I., Wegmann, K.W., Jones-Brando, L., Yolken, R.H., Bordón, C., Charman, S.A., Katneni, K., Schultz, T., et al. (2012). Endochin-like quinolones are highly efficacious against acute and latent experimental toxoplasmosis. Proceedings of the National Academy of Sciences of the United States of America 109, 15936-15941.

Doggett, J.S., Ojo, K.K., Fan, E., Maly, D.J., and Van Voorhis, W.C. (2014). Bumped kinase inhibitor 1294 treats established Toxoplasma gondii infection. Antimicrobial agents and chemotherapy 58, 3547-3549.

Donald, R.G., Allocco, J., Singh, S.B., Nare, B., Salowe, S.P., Wiltsie, J., and Liberator, P.A. (2002). Toxoplasma gondii cyclic GMP-dependent kinase: chemotherapeutic targeting of an essential parasite protein kinase. Eukaryot. Cell 1, 317-328.

Dou, Z., McGovern, O.L., Di Cristina, M., and Carruthers, V.B. (2014). Toxoplasma gondii ingests and digests host cytosolic proteins. mBio 5, e01188-01114.

Dubey, J.P. (1980). Mouse pathogenicity of Toxoplasma gondii isolated from a goat. Am. J. Vet. Res. 41, 427-429.

Dubey, J.P. (1988). Long-term persistence of Toxoplasma gondii in tissues of pigs inoculated with T gondii oocysts and effect of freezing on viability of tissue cysts in pork. Am. J. Vet. Res. 49, 910-913.

Dubey, J.P. (1998). Re-examination of resistance of Toxoplasma gondii tachyzoites and bradyzoites to pepsin and trypsin digestion. Parasitology 116 ( Pt 1), 43-50.

Dubey, J.P., Kotula, A.W., Sharar, A., Andrews, C.D., and Lindsay, D.S. (1990). Effect of high temperature on infectivity of Toxoplasma gondii tissue cysts in pork. Int. J. Parasitol. 76, 201-204.

Dunay, I.R., Gajurel, K., Dhakal, R., Liesenfeld, O., and Montoya, J.G. (2018). Treatment of Toxoplasmosis: Historical Perspective, Animal Models, and Current Clinical Practice. Clin. Microbiol. Rev. 31.

Ferguson, D.J. (2004). Use of molecular and ultrastructural markers to evaluate stage conversion of Toxoplasma gondii in both the intermediate and definitive host. Int. J. Parasitol. 34, 347-360.

Ferguson, D.J., Huskinson-Mark, J., Araujo, F.G., and Remington, J.S. (1994a). A morphological study of chronic cerebral toxoplasmosis in mice: comparison of four different strains of Toxoplasma gondii. Parasitol. Res. 80, 493-501.

Ferguson, D.J., Huskinson-Mark, J., Araujo, F.G., and Remington, J.S. (1994b). An ultrastructural study of the effect of treatment with atovaquone in brains of mice chronically infected with the ME49 strain of Toxoplasma gondii. Int. J. Exp. Pathol. 75, 111-116.

Ferguson, D.J., and Hutchison, W.M. (1987). An ultrastructural study of the early development and tissue cyst formation of Toxoplasma gondii in the brains of mice. Parasitol. Res. 73, 483-491.

Ferreira-da-Silva Mda, F., Takacs, A.C., Barbosa, H.S., Gross, U., and Lüder, C.G. (2009). Primary skeletal muscle cells trigger spontaneous Toxoplasma gondii tachyzoite-to-bradyzoite conversion at higher rates than fibroblasts. Int. J. Med. Microbiol. 299, 381-388.

Ferreira da Silva Mda, F., Barbosa, H.S., Gross, U., and Lüder, C.G. (2008). Stress-related and spontaneous stage differentiation of Toxoplasma gondii. Mol. Biosyst. 4, 824-834.

Fox, B.A., and Bzik, D.J. (2002). De novo pyrimidine biosynthesis is required for virulence of Toxoplasma gondii. Nature 415, 926-929.

Fox, B.A., Falla, A., Rommereim, L.M., Tomita, T., Gigley, J.P., Mercier, C., Cesbron-Delauw, M.F., Weiss, L.M., and Bzik, D.J. (2011). Type II Toxoplasma gondii KU80 knockout strains enable functional analysis of genes required for cyst development and latent infection. Eukaryot. Cell 10, 1193-1206.

Fox, B.A., Gigley, J.P., and Bzik, D.J. (2004). Toxoplasma gondii lacks the enzymes required for de novo arginine biosynthesis and arginine starvation triggers cyst formation. Int. J. Parasitol. 34, 323-331.

Fux, B., Nawas, J., Khan, A., Gill, D., Su, C., and Sibley, L.D. (2007). Toxoplasma gondii Strains Defective in Oral Transmission Are Also Defective in Developmental Stage Differentiation. Infection and immunity. 75, 2580-2590.

Gross, D.N., van den Heuvel, A.P., and Birnbaum, M.J. (2008). The role of FoxO in the regulation of metabolism. Oncogene 27, 2320-2336.

Gross, U., Bormuth, H., Gaissmaier, C., Dittrich, C., Krenn, V., Bohne, W., and Ferguson, D.J. (1995). Monoclonal rat antibodies directed against Toxoplasma gondii suitable for studying tachyzoite-bradyzoite interconversion in vivo. Clin. Diagn. Lab. Immunol. 2, 542-548.

Guimarães, E.V., Carvalho, L.d., and Barbosa, H.S. (2009). Interaction and cystogenesis of Toxoplasma gondii within skeletal muscle cells in vitro. Memórias do Instituto Oswaldo Cruz 104, 170-174.

Guimaraes, E.V., de Carvalho, L., and Barbosa, H.S. (2008). Primary culture of skeletal muscle cells as a model for studies of Toxoplasma gondii cystogenesis. Int. J. Parasitol. 94, 72-83.

Guo, Z.-G., Gross, U., and Johnson, A.M. (1997). Toxoplasma gondii virulence markers identified by random amplified polymorphic DNA polymerase chain reaction. Parasitology Research 83, 458-463.

Haug, K., Cochrane, K., Nainala, V.C., Williams, M., Chang, J., Jayaseelan, K.V., and O'Donovan, C. (2020). MetaboLights: a resource evolving in response to the needs of its scientific community. Nucleic acids research 48, D440-d444.

Hegewald, J., Gross, U., and Bohne, W. (2013). Identification of dihydroorotate dehydrogenase as a relevant drug target for 1-hydroxyquinolones in Toxoplasma gondii. Mol. Biochem. Parasitol. 190, 6-15.

Hortua Triana, M.A., Huynh, M.H., Garavito, M.F., Fox, B.A., Bzik, D.J., Carruthers, V.B., Loffler, M., and Zimmermann, B.H. (2012). Biochemical and molecular characterization of the pyrimidine biosynthetic enzyme dihydroorotate dehydrogenase from Toxoplasma gondii. Mol Biochem. Parasitol. 184, 71-81.

Huang, W., Ojo, K.K., Zhang, Z., Rivas, K., Vidadala, R.S., Scheele, S., DeRocher, A.E., Choi, R., Hulverson, M.A., Barrett, L.K., et al. (2015). SAR Studies of 5-Aminopyrazole-4-carboxamide Analogues as Potent and Selective Inhibitors of Toxoplasma gondii CDPK1. ACS Med. Chem. Letter 6, 1184-1189.

Huynh, M.-H., and Carruthers, V.B. (2009). Tagging of endogenous genes in a Toxoplasma gondii strain lacking Ku80. Eukaryotic cell 8, 530-539.

Jeffers, V., Tampaki, Z., Kim, K., and Sullivan, W.J., Jr. (2018). A latent ability to persist: differentiation in Toxoplasma gondii. Cell Mol. Life Sci. 75, 2355-2373.

John, B., Harris, T.H., Tait, E.D., Wilson, E.H., Gregg, B., Ng, L.G., Mrass, P., Roos, D.S., Dzierszinski, F., Weninger, W., et al. (2009). Dynamic Imaging of CD8(+) T cells and dendritic cells during infection with Toxoplasma gondii. PLoS pathogens 5, e1000505.

Krishnan, A., Kloehn, J., Lunghi, M., Chiappino-Pepe, A., Waldman, B.S., Nicolas, D., Varesio, E., Hehl, A., Lourido, S., Hatzimanikatis, V., et al. (2020). Functional and Computational Genomics Reveal Unprecedented Flexibility in Stage-Specific Toxoplasma Metabolism. Cell Host Microbe 27, 290-306.e211.

Kumar, A., Kumar, Y., Sevak, J.K., Kumar, S., Kumar, N., and Gopinath, S.D. (2020). Metabolomic analysis of primary human skeletal muscle cells during myogenic progression. Sci. Rep. 10, 11824.

Laue, M. (2010). Electron microscopy of viruses. Methods in cell biology 96, 1-20.

Lopatkin, A.J., Stokes, J.M., Zheng, E.J., Yang, J.H., Takahashi, M.K., You, L., and Collins, J.J. (2019). Bacterial metabolic state more accurately predicts antibiotic lethality than growth rate. Nat. microbiology 4, 2109-2117.

Lüder, C.G.K., and Rahman, T. (2017). Impact of the host on Toxoplasma stage differentiation. Microb. Cell 4, 203-211.

Luft, B.J., Brooks, R.G., Conley, F.K., McCabe, R.E., and Remington, J.S. (1984). Toxoplasmic encephalitis in patients with acquired immune deficiency syndrome. Jama 252, 913-917.

MacRae, J.I., Sheiner, L., Nahid, A., Tonkin, C., Striepen, B., and McConville, M.J. (2012). Mitochondrial metabolism of glucose and glutamine is required for intracellular growth of Toxoplasma gondii. Cell Host Microbe 12, 682-692.

Mahamed, D.A., Mills, J.H., Egan, C.E., Denkers, E.Y., and Bynoe, M.S. (2012). CD73-generated adenosine facilitates Toxoplasma gondii differentiation to long-lived tissue cysts in the central nervous system. Proceedings of the National Academy of Sciences of the United States of America 109, 16312-16317.

Malinska, D., Kudin, A.P., Bejtka, M., and Kunz, W.S. (2012). Changes in mitochondrial reactive oxygen species synthesis during differentiation of skeletal muscle cells. Mitochondrion 12, 144-148.

Matsuda, R., Uchitomi, R., Oyabu, M., Hatazawa, Y., and Kamei, Y. (2019). Metabolomic analysis of C2C12 myoblasts induced by the transcription factor FOXO1. FEBS letters 593, 1303-1312.

Matta, S.K., Olias, P., Huang, Z., Wang, Q., Park, E., Yokoyama, W.M., and Sibley, L.D. (2019). Toxoplasma gondii effector TgIST blocks type I interferon signaling to promote infection. Proceedings of the National Academy of Sciences of the United States of America 116, 17480-17491.

Mayoral, J., Di Cristina, M., Carruthers, V.B., and Weiss, L.M. (2020). Toxoplasma gondii: Bradyzoite Differentiation In Vitro and In Vivo. Methods Mol. Biol. 2071, 269-282.

Metsalu, T., and Vilo, J. (2015). ClustVis: a web tool for visualizing clustering of multivariate data using Principal Component Analysis and heatmap. Nucleic acids research 43, W566-570.

Murata, Y., Sugi, T., Weiss, L.M., and Kato, K. (2017). Identification of compounds that suppress Toxoplasma gondii tachyzoites and bradyzoites. PLoS One 12, e0178203.

Olson, W.J., Martorelli Di Genova, B., Gallego-Lopez, G., Dawson, A.R., Stevenson, D., Amador-Noguez, D., and Knoll, L.J. (2020). Dual metabolomic profiling uncovers Toxoplasma manipulation of the host metabolome and the discovery of a novel parasite metabolic capability. PLoS pathogens 16, e1008432.

Painter, H.J., Morrisey, J.M., Mather, M.W., and Vaidya, A.B. (2007). Specific role of mitochondrial electron transport in blood-stage Plasmodium falciparum. Nature 446, 88-91.

Parker, K.E.R., Fairweather, S.J., Rajendran, E., Blume, M., McConville, M.J., Bröer, S., Kirk, K., and van Dooren, G.G. (2019). The tyrosine transporter of Toxoplasma gondii is a member of the newly defined apicomplexan amino acid transporter (ApiAT) family. PLoS pathogens 15, e1007577.

Pittman, K.J., Aliota, M.T., and Knoll, L.J. (2014). Dual transcriptional profiling of mice and Toxoplasma gondii during acute and chronic infection. BMC genomics 15, 806.

Radke, J.R., Donald, R.G., Eibs, A., Jerome, M.E., Behnke, M.S., Liberator, P., and White, M.W. (2006). Changes in the expression of human cell division autoantigen-1 influence Toxoplasma gondii growth and development. PLoS pathogens 2, e105.

Roos, D.S. (1993). Primary structure of the dihydrofolate reductase-thymidylate synthase gene from Toxoplasma gondii. J. Biol. Chem 268, 6269-6280.

Sabin, A.B. (1941). Toxoplasmic Encephalitis In Children. Jama 116, 801-807.

Saleh, A., Friesen, J., Baumeister, S., Gross, U., and Bohne, W. (2007). Growth inhibition of Toxoplasma gondii and Plasmodium falciparum by nanomolar concentrations of 1-hydroxy-2-dodecyl-4(1H)quinolone, a high-affinity inhibitor of alternative (type II) NADH dehydrogenases. Antimicrob. Agents Chemother 51, 1217-1222.

Saunders, E.C., Ng, W.W., Kloehn, J., Chambers, J.M., Ng, M., and McConville, M.J. (2014). Induction of a stringent metabolic response in intracellular stages of Leishmania mexicana leads to increased dependence on mitochondrial metabolism. PLoS pathogens 10, e1003888.

Scheele, S., Geiger, J.A., DeRocher, A.E., Choi, R., Smith, T.R., Hulverson, M.A., Vidadala, R.S.R., Barrett, L.K., Maly, D.J., Merritt, E.A., et al. (2018). Toxoplasma Calcium-Dependent Protein Kinase 1 Inhibitors: Probing Activity and Resistance Using Cellular Thermal Shift Assays. Antimicrob. Agents Chemother 62.

Schneider, C.A., Rasband, W.S., and Eliceiri, K.W. (2012). NIH Image to ImageJ: 25 years of image analysis. Nat. Methods 9, 671-675.

Shiomi, K., Kiyono, T., Okamura, K., Uezumi, M., Goto, Y., Yasumoto, S., Shimizu, S., and Hashimoto, N. (2011). CDK4 and cyclin D1 allow human myogenic cells to recapture growth property without compromising differentiation potential. Gene Ther. 18, 857-866.

Shukla, A., Olszewski, K.L., Llinas, M., Rommereim, L.M., Fox, B.A., Bzik, D.J., Xia, D., Wastling, J., Beiting, D., Roos, D.S., et al. (2018). Glycolysis is important for optimal asexual growth and formation of mature tissue cysts by Toxoplasma gondii. Int. J. Parasitol. 48, 955-968.

Sibley, L.D., Mordue, D.G., Su, C., Robben, P.M., and Howe, D.K. (2002). Genetic approaches to studying virulence and pathogenesis in Toxoplasma gondii. Philos. Trans. R. Soc. Lond. B. Biol. Sci. 357, 81-88.

Singh, U., Brewer, J.L., and Boothroyd, J.C. (2002). Genetic analysis of tachyzoite to bradyzoite differentiation mutants in Toxoplasma gondii reveals a hierarchy of gene induction. Mol. Microbiol. 44, 721-733.

Smith, D., Kannan, G., Coppens, I., Wang, F., Nguyen, H.M., Cerutti, A., Schultz, T.L., Rimple, P.A., Di Cristina, M., Besteiro, S., et al. (2020). TgATG9 is critical for autophagy and long-term persistence in tissue cysts. bioRxiv 2020.2005.2013.093401.

Soete, M., Camus, D., and Dubremetz, J.F. (1994). Experimental induction of bradyzoite-specific antigen expression and cyst formation by the RH strain of Toxoplasma gondii in vitro. Exp. Parasitol. 78, 361-370.

Speer, C.A., Dubey, J.P., McAllister, M.M., and Blixt, J.A. (1999). Comparative ultrastructure of tachyzoites, bradyzoites, and tissue cysts of Neospora caninum and Toxoplasma gondii. Int. J. Parasitol. 29, 1509-1519.

Sugi, T., Tu, V., Ma, Y., Tomita, T., and Weiss, L.M. (2017). Toxoplasma gondii Requires Glycogen Phosphorylase for Balancing Amylopectin Storage and for Efficient Production of Brain Cysts. mBio 8.

Sullivan, W.J., Jr., Smith, A.T., and Joyce, B.R. (2009). Understanding mechanisms and the role of differentiation in pathogenesis of Toxoplasma gondii: a review. Mem. Inst. Oswaldo Cruz 104, 155-161.

Swierzy, I.J., and Lüder, C.G.K. (2015). Withdrawal of skeletal muscle cells from cell cycle progression triggers differentiation of Toxoplasma gondii towards the bradyzoite stage. Cellular Microbiology 17, 2-17.

Tenter, A., Heckeroth, A., and Weiss, L. (2000). Toxoplasma gondii: From animals to humans. Int. J. Parasitol. 30, 1217-1258.

Tomavo, S., and Boothroyd, J.C. (1995). Interconnection between organellar functions, development and drug resistance in the protozoan parasite, Toxoplasma gondii. Int. J. Parasitol. 25, 1293-1299.

Watts, E., Zhao, Y., Dhara, A., Eller, B., Patwardhan, A., and Sinai, A.P. (2015). Novel Approaches Reveal that Bradyzoites within Tissue Cysts Are Dynamic and Replicating Entities. mBio 6, e01155-01115.

Weilhammer, D.R., Iavarone, A.T., Villegas, E.N., Brooks, G.A., Sinai, A.P., and Sha, W.C. (2012). Host metabolism regulates growth and differentiation of Toxoplasma gondii. Int. J. Parasitol. 42, 947-959.

Winzer, P., Muller, J., Aguado-Martinez, A., Rahman, M., Balmer, V., Manser, V., Ortega-Mora, L.M., Ojo, K.K., Fan, E., Maly, D.J., et al. (2015). In Vitro and In Vivo Effects of the Bumped Kinase Inhibitor 1294 in the Related Cyst-Forming Apicomplexans Toxoplasma gondii and Neospora caninum. Antimicrob Agents Chemother 59, 6361-6374.

Xia, N., Zhou, T., Liang, X., Ye, S., Zhao, P., Yang, J., Zhou, Y., Zhao, J., and Shen, B. (2018). A Lactate Fermentation Mutant of Toxoplasma Stimulates Protective Immunity Against Acute and Chronic Toxoplasmosis. Front. Imm. 9, 1814.

Yap, G.S., Scharton-Kersten, T., Ferguson, D.J., Howe, D., Suzuki, Y., and Sher, A. (1998). Partially protective vaccination permits the development of latency in a normally virulent strain of Toxoplasma gondii. Infect. Immun. 66, 4382-4388.

Fig. 1

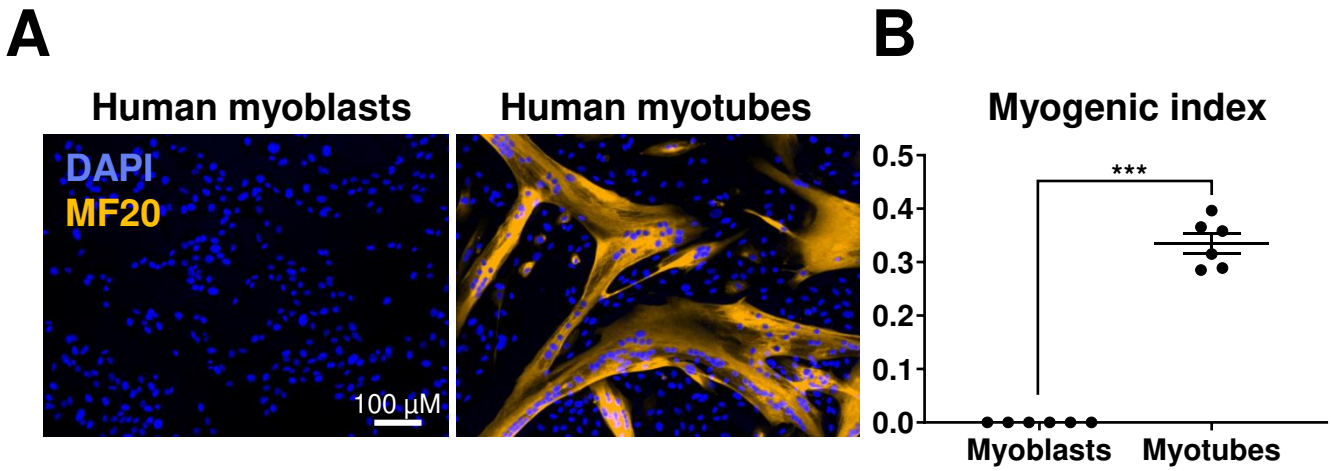

Fig. 2

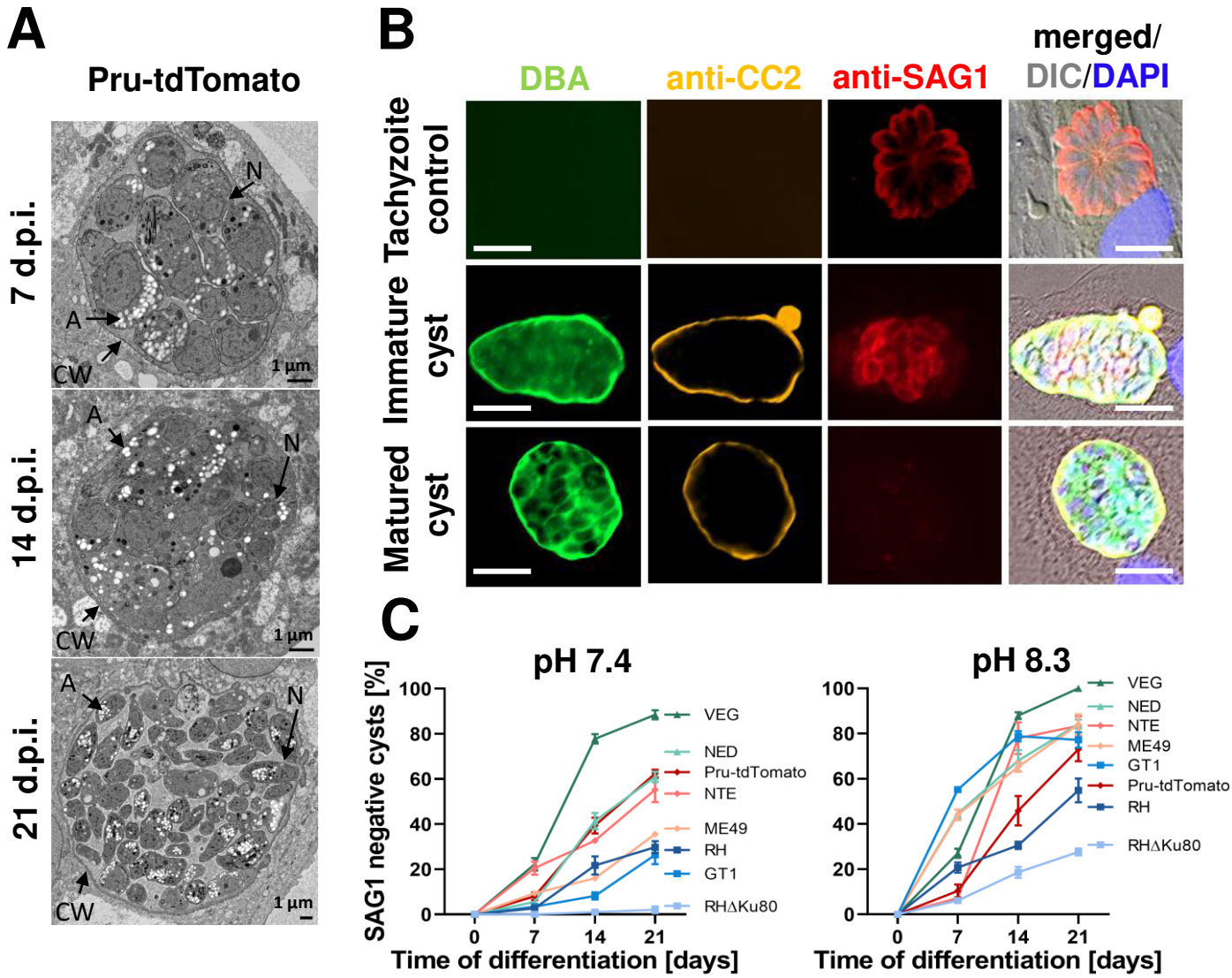

# Fig. 3

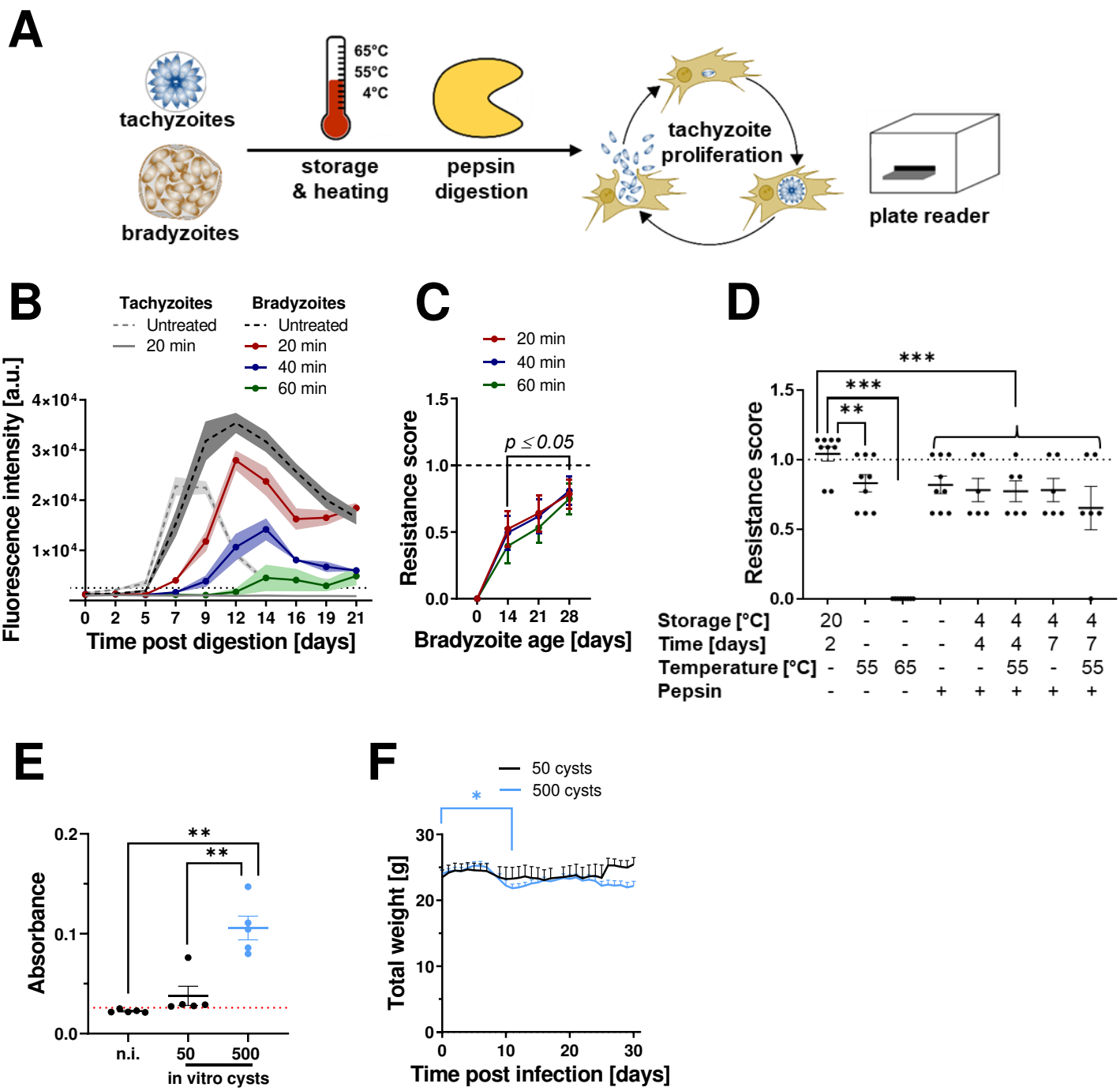

Fig. 4

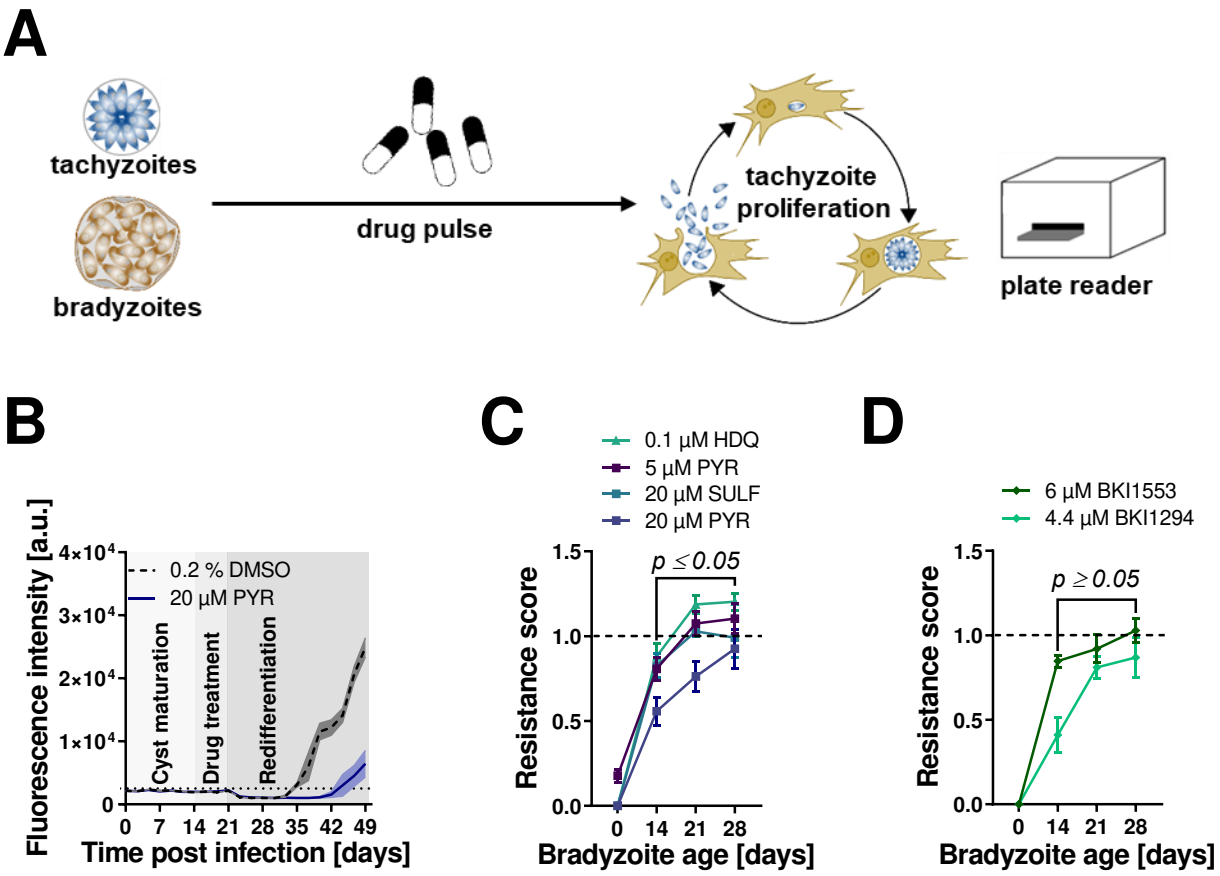

# Fig. 5

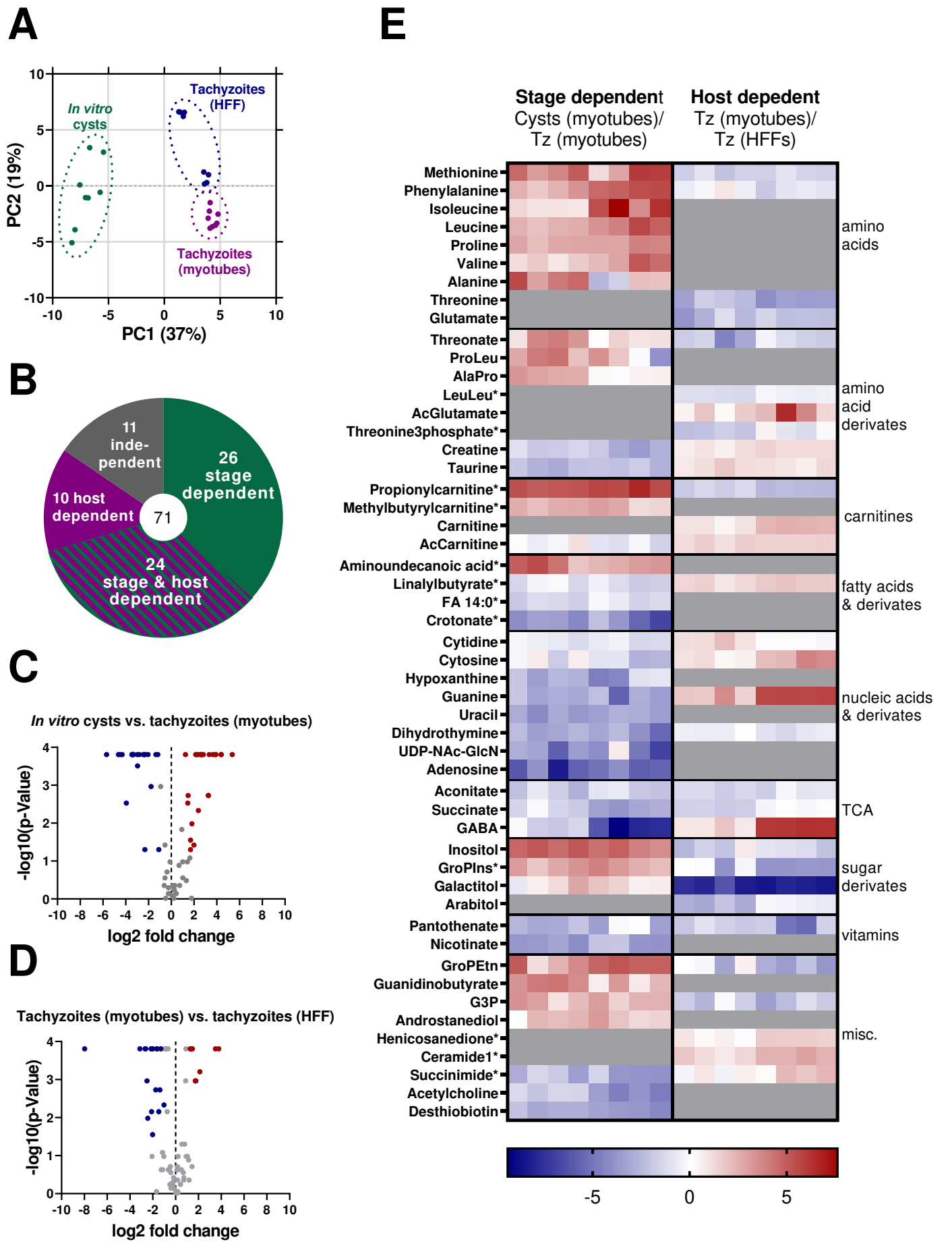

# Fig. 6

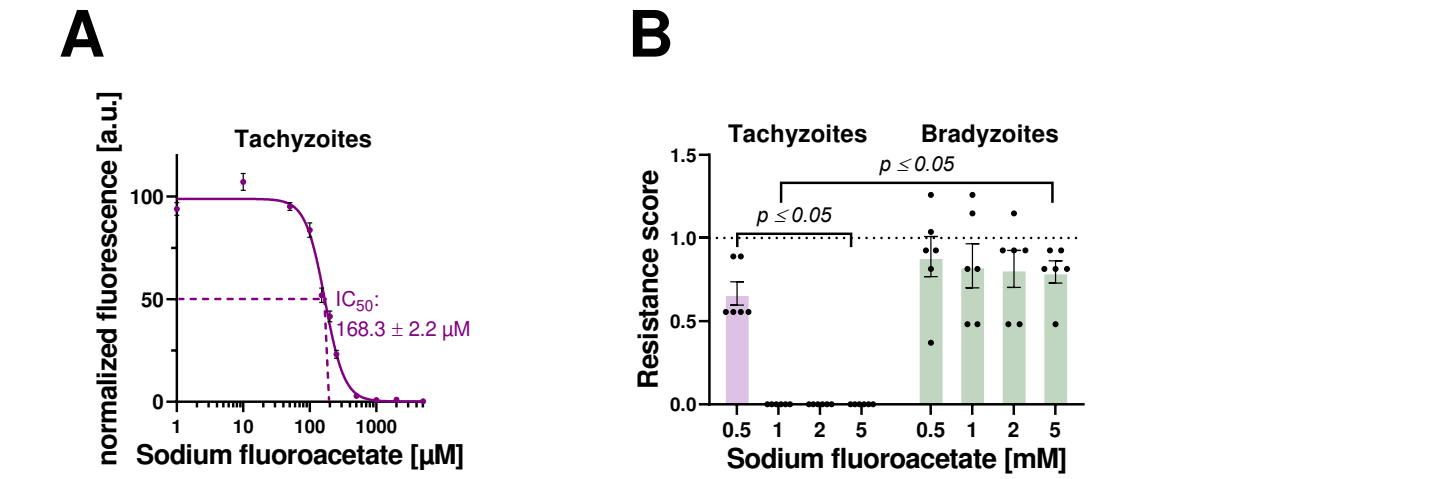

# Fig. S1

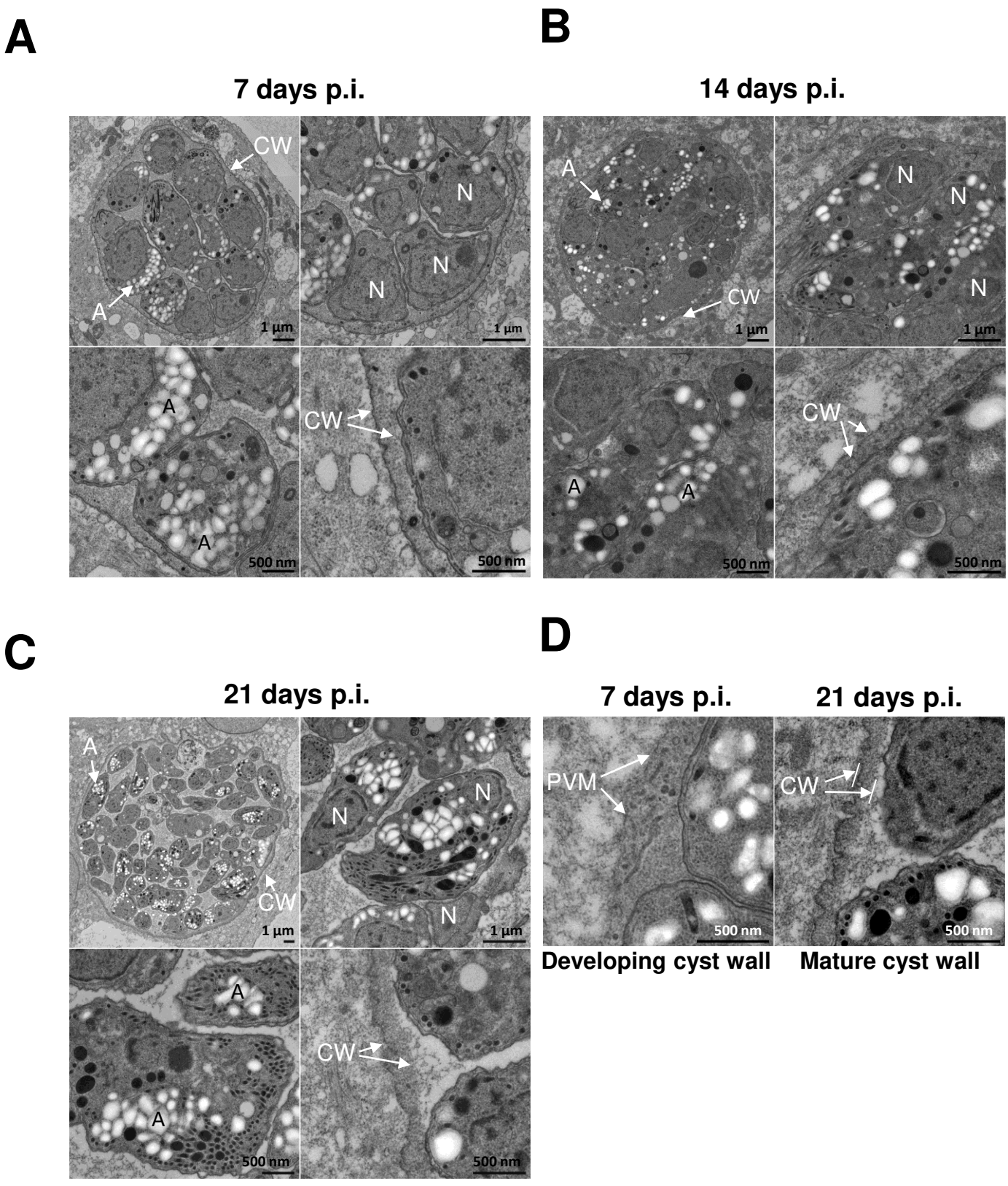

**Fig. S2**

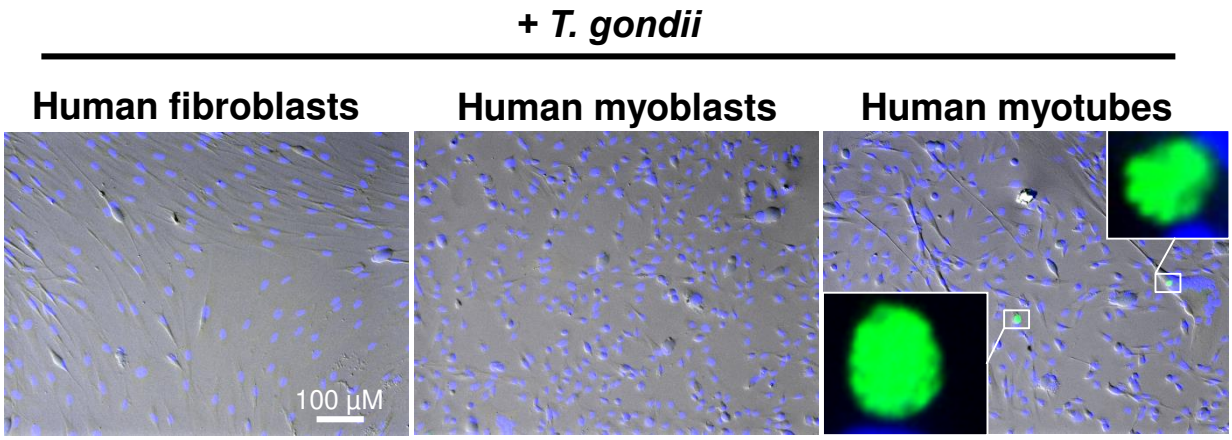

# Fig. S3

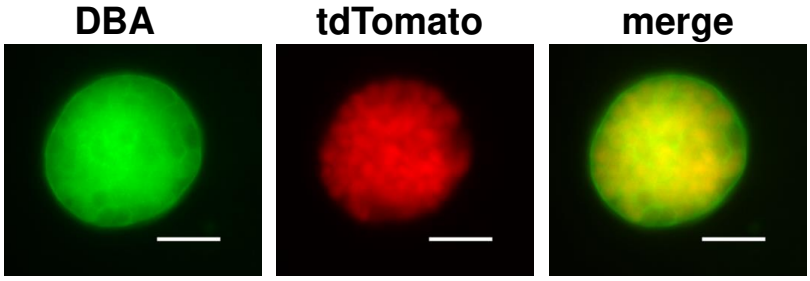

# Fig. S4

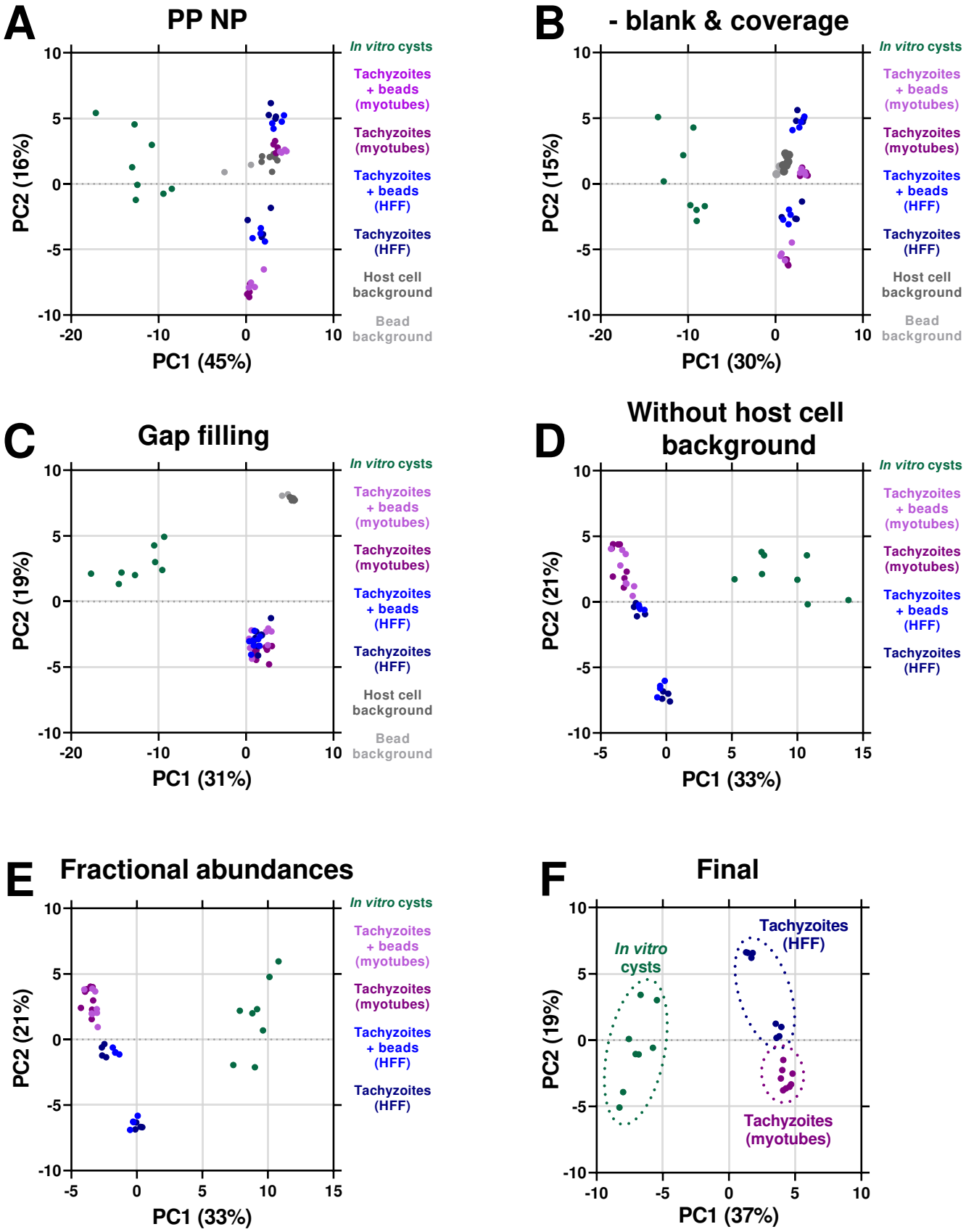

# Fig. S5

| Name | Gene ID | Acute infection (10 d.p.i.) | Chronic infection (28 d.p.i.) | chronic/acute |
|---|---|---|---|---|
| TgAT | TGME49_244440 | 75.64 | 3.5 | 0.05 |
| TgAT1 high affinity | TGME49_233130 | 27.87 | 76.36 | 2.74 |
| TgAT2 high affinity | TGME49_288540 | 30.4 | 36.33 | 1.20 |
| TgApiAT5-3 | TGME49_257530 | 1037.34 | 283.94 | 0.27 |
| TgApiAT6-3 | TGME49_249580 | 24.05 | 8.7 | 0.36 |
| TgApiAT5-1 | TGME49_248610 | 14.27 | 6.89 | 0.48 |
| TgApiAT7-1 | TGME49_263230 | 49.22 | 25.71 | 0.52 |
| TgApiAT1 | TGME49_215490 | 83.03 | 45.73 | 0.55 |
| TgApiAT6-2 | TGME49_290860 | 30.76 | 16.92 | 0.55 |
| TgApiAT3-1 | TGME49_318150 | 13.73 | 8.06 | 0.59 |
| TgApiAT7-2 | TGME49_263260 | 71.19 | 44.06 | 0.62 |
| TgApiAT2 | TGME49_320020 | 38.62 | 24.4 | 0.63 |
| TgApiAT3-2 | TGME49_248420 | 41.93 | 28.78 | 0.69 |
| TgApiAT6-1 | TGME49_240810 | 40.39 | 28.78 | 0.71 |
| TgApiAT5-5 | TGME49_293420 | 0.01 | 0.01 | 1.00 |
| TgApiAT5-6 | TGME49_293425 | 0.01 | 0.01 | 1.00 |
| TgApiAT3-3 | TGME49_220600 | 24.69 | 26.66 | 1.08 |
| TgApiAT5-4 | TGME49_216710 | 4.26 | 9.05 | 2.12 |
| TgApiAT5-2 | TGME49_205520 | 0.01 | 2.11 | 211.00 |